Available online at www.sciencedirect.com
SCIENCE DIRECT
Journal of Catalysis 233 (2005) 147–165
JOURNAL OF CATALYSIS
www.elsevier.com/locate/jcat

Dehydrogenation of isopropyl alcohol on carbon-supported Pt and Cu–Pt catalysts

R.M. Rioux, M.A. Vannice *

Department of Chemical Engineering, Pennsylvania State University, University Park, PA 16802, USA

Received 9 February 2005; revised 12 April 2005; accepted 15 April 2005

Available online 26 May 2005

Abstract

The kinetics of isopropyl alcohol (IPA) dehydrogenation over carbon-supported Pt and three bimetallic Cu–Pt catalysts were examined and compared with previous results for carbon-supported Cu. Adsorption of H_2 and CO, dissociative chemisorption of N_2O, and the titration of adsorbed O atoms by H_2 and CO were used to determine surface compositions and metal dispersion. Monometallic platinum catalysts had a higher specific activity than monometallic Cu catalysts and the bimetallic catalysts; for example, at 448 K and 14 Torr IPA, for an activated carbon heat treated at 1223 K as the support, the turnover frequency (TOF) on the Pt catalyst was 0.11 s^{-1}, the TOF on the Cu catalyst was 0.020 s^{-1}, and the TOFs on the three bimetallic catalysts were between 0.006 and 0.043 s^{-1}. Reaction orders were typically between 0 and $\frac{1}{2}$ for IPA and slightly negative for acetone and H_2. Increasing the Cu loading reduced the number of surface Pt atoms, and the kinetic behavior became similar to that of monometallic copper catalysts. The apparent activation energy for acetone production from IPA on Pt/C was 6.8 kcal mol^{-1}, compared with 21 kcal mol^{-1} for the monometallic Cu/C catalysts. Apparent activation energies for the Cu–Pt/C catalysts (7–9 kcal mol^{-1}) were comparable to those of Pt/C at lower temperatures and decreased further to $\sim$ 3 kcal mol^{-1} above 443 K. This decrease is not due to diffusional limitations and can be explained by a decrease in the surface coverage of IPA. A Langmuir–Hinshelwood model invoking cleavage of the alcohol O–H bond to form a surface isopropoxide species as the rate-determining step fit the data well and accounted for the shift in the apparent activation energy. Physically meaningful values of enthalpies and entropies of adsorption were obtained from the fitting parameters contained in the L-H rate expression. Additional evidence for adsorbed IPA and acetone was provided by infrared spectra of the catalysts obtained under reaction conditions.

Keywords: Isopropanol dehydrogenation; Dehydrogenation of alcohols; Pt/C and Pt–Cu/C catalysts; Kinetics of dehydrogenation; Carbon supports

1. Introduction

The replacement of copper chromite systems with more environmentally benign copper catalysts, such as carbon-supported Cu, is of current interest because of the prohibition of chromite disposal in landfills by the EPA. Cu is highly selective for alcohol dehydrogenation but suffers from low activity and a propensity to sinter; thus, the addition of a second metal may not only increase dehydrogenation activity and catalyst lifetime and still maintain high selectivity, but also facilitate reduction of the Cu precursor to metallic Cu. The bimetallic Cu–Pt/C catalysts investigated here were prepared by the addition of Cu to a prereduced Pt/C catalyst and then characterized by chemisorption, X-ray diffraction (XRD), X-ray photoelectron spectroscopy (XPS), transmission electron microscopy (TEM), and temperature-programmed reduction (TPR). The addition of a group IB metal such as copper to a Group VIII metal, with its partially filled *d*-bands, might be expected to reduce the catalytic activity for dehydrogenation [1,2]; such a decrease could occur in these bimetallic catalysts relative to monometallic Cu and Pt systems. Conversely, the activity of a bimetallic Cu–Pt catalyst could increase relative to Cu alone because of the high affinity of hydrogen for Pt relative to copper. This would provide a mechanism where the Pt surface acts as a sink for H and facilitates H_2 desorption, thereby freeing the

* Corresponding author.
E-mail address: mavche@engr.psu.edu (M.A. Vannice).

0021-9517/$ – see front matter
doi:10.1016/j.jcat.2005.04.020

Cu surface to adsorb and dissociate isopropyl alcohol (IPA). This role of Pt in a Group IB bimetallic catalyst has been postulated previously [3], but for this to enhance activity, one would anticipate that H_2 desorption is rate-determining. To better understand the behavior of platinum in dehydrogenation reactions, Pt/C catalysts were studied to complement previous work with Cu/C catalysts [4] and to allow appropriate comparisons between the two monometallic catalysts.

The surface chemistry of alcohols on single crystals of various metals has been studied [5–12]; however, little work has been conducted with single crystals of Cu, a metal highly selective for alcohol dehydrogenation, although oxygen-covered Cu single crystals have been investigated [13–15]. In most of these investigations, evidence has strongly suggested that alcohol dehydrogenation occurs via an alkoxide intermediate, which has been identified by a variety of surface science techniques. Consequently, an alkoxide species is a likely intermediate during alcohol dehydrogenation on metal surfaces, and evidence has indicated the presence of such a surface species on dispersed metal catalysts [16–18]. Kinetic modeling of this reaction on a Cu/SiO_2 catalyst has suggested that the dehydrogenation of IPA occurs through an isopropoxide intermediate and that the rate-determining step (RDS) involves further dehydrogenation of this isopropoxide species to acetone [17]. However, there is no general consensus about the RDS in these alcohol dehydrogenation reactions [4,19–23], and, should a RDS exist, it may be dependent on the structure of the alcohol, the type of metal surface, and the reaction conditions.

Reaction pathways for alcohol dehydrogenation have been discussed primarily in the surface science literature related to monometallic single crystals, and considerably less work has been conducted on the kinetics of alcohol dehydrogenation over any type of bimetallic catalysts. In alcohol formation, a synergistic effect between Cu and Zn for methanol synthesis has been documented by a number of researchers [24–28], and it is known that the rate of alcohol dehydrogenation is metal specific [1,2]. However, the effect of the metals chosen and their composition in bimetallic systems are poorly understood with regard to alcohol dehydrogenation chemistry, although there are some examples involving the addition of zinc to a Cu/SiO_2 catalyst [23] and the addition of vanadium to Cu–Zn catalysts [29]. The one study reported on the reaction mechanism of alcohol dehydrogenation on carbon-supported copper catalysts showed that the reaction appears to be relatively structure insensitive and that a Langmuir–Hinshelwood kinetic model with the removal of the hydroxyl hydrogen as the RDS accurately fit the data and provided meaningful thermodynamic values for the fitting parameters [4]. IPA dehydrogenation over Pt and bimetallic Cu–Pt catalysts has not been examined, so a detailed kinetic and mechanistic analysis of this reaction over these catalysts was undertaken. These catalysts were characterized by XRD, TEM, and a variety of chemisorption methods, some just recently developed, to determine overall metal dispersion and surface composition.

2. Experimental

2.1. Catalysts

The carbon used in the study has been described previously [30], but a brief summary is given here. Activated carbon (Norit SX-1) was obtained from the Norit Corporation; it had a specific surface area of 800 $m^2\,g^{-1}$ and a pore volume of ~ 0.5 $cm^3\,g^{-1}$. This carbon is referred to as AC-ASIS, and its major impurities were Si, S, Na, and Al [4,31]. After this carbon was washed in refluxing nitric acid (12 N, J.T. Baker) at 363 K for 12 h, its surface was rich in oxygen-containing functional groups, and its surface area was 616 $m^2\,g^{-1}$. This carbon is designated AC-HNO_3. We produced a high-temperature-treated carbon (AC-HTT-H_2) with a hydrophobic surface by heating the ASIS carbon to 1223 K in flowing H_2 for 6 h. The final material had a BET surface area of 1137 $m^2\,g^{-1}$.

The carbon-supported catalysts were prepared by a wet impregnation technique utilizing 0.5 $cm^3\,g^{-1}$ of aqueous metal salt solution with the metal precursors copper nitrate, $Cu(NO_3)_2 \cdot xH_2O$ (99.999%, Aldrich), and chloroplatinic acid, $H_2PtCl_6 \cdot xH_2O$ (99.995%, Aldrich). Aqueous solutions of appropriate composition were added dropwise to a carbon sample that was continuously stirred, and the catalysts were dried overnight at 393 K in air. Before further characterization, catalyst samples were heated at either 473 or 573 K under 50 sccm He (1 atm) for 1 h and then reduced in 50 sccm H_2 (1 atm) at the same temperature for 4 h.

Bimetallic Cu–Pt samples were prepared with a 1% Pt catalyst that had been heated under He for 1 h and then reduced for 1 h at 673 K, followed by room-temperature passivation in 1% O_2/He. After impregnation with a Cu solution to give Cu loadings of 0.5, 1, or 5 wt%, these catalysts were dried overnight at 393 K. Before use, these catalysts were reduced as stated earlier. Actual Cu and Pt loadings were determined by inductively coupled plasma emission-mass spectrometry at Pennsylvania State University [31]. We cleaned ultra-high-purity (UHP) Pt powder (99.999%, Alfa Aesar) by heating it at 573 K for 15 min in 10% O_2/He to remove any surface contaminants by oxidation before normal catalyst pretreatment.

2.2. Catalyst characterization

Monometallic Cu catalysts were characterized by selective chemisorption techniques and X-ray diffraction (XRD) as described previously [4]. Pt/C catalysts were characterized by H_2, CO, and oxygen chemisorption (via N_2O decomposition). Volumetric chemisorption measurements were conducted in a stainless-steel apparatus equipped with a mechanical pump (Edwards E1M5) and a diffusion pump (Edwards Diffstak MK2), which maintained a vacuum below 10^{-6} in the chemisorption cell. The dual isotherm method, with a 1-h evacuation between isotherms, was used to measure total and reversible H_2 and CO adsorption and titration

uptakes at 300 K, with irreversible adsorption represented by the difference between the two uptakes. The decomposition of N_2O at 363 K on catalyst samples (7–10 mg) was measured gravimetrically in a thermal gravimetric analysis system (Perkin-Elmer TGS-2) with an instrumental sensitivity of 0.1 μg [32,33].

Titration of chemisorbed oxygen at 300 K by CO and H_2 [34], as well as other more standard chemisorption methods, was used to determine the overall dispersion and surface composition in these bimetallic Cu–Pt catalysts. Four separate experiments were conducted on each sample. First, after appropriate reduction the sample (ca. 400 mg) was cooled to room temperature and both total and reversible H_2 isotherms were measured. Second, the catalyst was reheated to 573 K under H_2 and held for 1 h, evacuated ($\sim$ 1 h) at 573 K, and cooled to 300 K, and total and reversible CO isotherms were collected. Third, the sample was re-reduced at 573 K under flowing H_2, evacuated for 1 h, and cooled to 363 K, where N_2O decomposition at 75 Torr N_2O was conducted, then after evacuation and cooling, the adsorbed O atoms were titrated with H_2 at 300 K. This experiment is designated as "N_2O–H_2 titration" [35]. Finally, after both total and reversible H_2 titration isotherms were obtained, the catalyst was re-reduced, evacuated, and cooled to 363 K, where 75 Torr N_2O was again introduced to the sample. Then, after decomposition, evacuation, and cooling to 300 K, the adsorbed O atoms were titrated with CO. This experiment is designated "N_2O–CO titration" [33]. A standard N_2O decomposition experiment at 75 Torr N_2O and 363 K was also conducted on a separate sample in the gravimetric apparatus [32]. These four sequential runs are summarized in Table 1, along with the information provided by each experiment.

X-ray photoelectron spectroscopy (XPS) measurements on bimetallic samples were obtained with a 5700 Physical Electronics LSci instrument with both a Mg and an Al X-ray source. Each sample was given the desired pretreatment and underwent the standard passivation procedure before handling in air for XPS measurements. Survey and regional (Cu energy region) scans were taken; the latter concentrated between 925 and 970 eV, since the $2p_{1/2}$ and $2p_{3/2}$ photoelectron lines for Cu are located at 933 and 953 eV, respectively.

Table 1
Bimetallic Cu–Pt catalyst characterization methodology

Run #	Experimental at 300 K	Designation	Information obtained
1	H_2 chemisorption on reduced sample	[H_T, H_{irr}]	Pt_s[a]
2	CO chemisorption on reduced sample	[CO_{irr}]	Pt_s[b]
3	H_2 titration after N_2O decomposition	[N_2O–H_2 titr.]	Pt_s
4	CO titration after N_2O decomposition	[N_2O–CO titr.]	$Pt_s + Cu^{+1}$

[a] Assuming no H spillover from Pt to Cu^0 and to the support.
[b] Assuming no Cu^{+1}.

Catalyst morphology and particle size measurements of Cu–Pt/AC-HTT-H_2 catalysts were determined by transmission electron microscopy (TEM). The microscope (Philips 420T) had an operating voltage of 130 kV. Reduced and passivated samples were ultrasonically dispersed in acetone and mounted on a 200-mesh copper lacy carbon grid (Electron Microscopy Sciences). On average, 150–200 particles were counted from bright-field images to determine statistically meaningful average particle sizes.

Temperature-programmed reduction (TPR) experiments were conducted with a glass microreactor connected to a temperature-programmed reduction setup with mass flow controllers and a thermal conductivity detector (TCD). Before measurement of the H_2 consumption, H_2O was removed from the gas flow by a zeolite trap. Heating rates varying from 5 to 20 K min^{-1} were used with a 30 cm^3 min^{-1} flow of 3% H_2 (Matheson, 99.999% purity)/97% Ar (Matheson, 99.999%). The heating rate was determined to have a minimal effect on the temperature where maximum reduction occurred; therefore only data for 10 K min^{-1} heating rates are shown.

2.3. Kinetic behavior

Kinetic studies of the vapor-phase dehydrogenation of IPA were conducted in a differential microreactor. He (MG Ind., 99.999%) and H_2 (MG Ind., 99.999%) flow rates were regulated with needle valves and monitored with Hasting-Raydist mass flow meters. We degassed isopropanol (Acros Organics, 99+% purity) either with three freeze/thaw cycles with liquid N_2 or by bubbling N_2 through it for 1 h. The IPA was pumped by a Sage Instruments (model 341A) syringe pump into a heated stainless-steel line, where it was vaporized. During experiments in which the effect of acetone on reaction kinetics was probed, acetone was fed to the inlet stream with a KD Scientific syringe pump. All lines before and after the reactor were heated to 393 K to prevent condensation, and the effluent composition was analyzed with a Hewlett-Packard 5890 gas chromatograph equipped with a Porapak T column (Supelco) [31].

Kinetic runs were conducted with 20–200 mg of catalyst that was pretreated in situ for 4 h at 473 or 573 K under 50 cm^3 (STP) min^{-1} H_2. After reduction, the catalyst was flushed with 25 cm^3 (STP) min^{-1} He for 30 min at the reduction temperature. Standard conditions for IPA dehydrogenation activity measurements were 14 Torr C_3H_7OH, no H_2 (balance He), and 448 K. The temperature dependencies for IPA dehydrogenation were determined over a temperature range of 423–473 K for monometallic platinum and 403–523 K for the bimetallic samples, and we obtained Arrhenius plots by varying the temperature in both an ascending and a descending order to verify reproducible activity and check for deactivation. Partial pressure studies of IPA, H_2, and acetone were conducted at four different

temperatures (433, 448, 458, and 473 K) for kinetic modeling purposes, with the use of the 1% Pt/AC-HTT-H_2 and the 5% Cu-1% Pt/AC-HTT-H_2 catalysts. For the bimetallic samples with lower Cu loadings, reaction orders were measured at 413, 423, 433, 448, 458, 473, and 493 K. During the IPA partial-pressure study, the IPA pressure ranged from 7 to 50 Torr (760 Torr = 1 atm), and during a H_2 pressure dependence study, the IPA pressure was constant at 14 Torr and the H_2 pressure was varied between 5 and 170 Torr. The dependence on acetone was determined at IPA and H_2 partial pressures of 14 and 0 Torr, respectively, while the acetone pressure was varied from 2 to 15 Torr. Data for the same experiment were obtained with different catalyst samples under identical conditions, and we compared these in order to calculate experimental uncertainty, which is ±5% (maximum) for the reaction order and ±3 kcal mol^{-1} for the apparent activation energy, and the reproducibility of turnover frequencies (TOFs) was > 90%. Additional details are provided elsewhere [31]. Kinetic performance was measured as activity in μmol s^{-1} g_{cat}^{-1}, which was then normalized per mole of surface Cu^0, Cu^{1+}, and Pt species to obtain a TOF, that is, molecule $site^{-1}$ s^{-1}, with a site representing any metal surface atom, M_s. Blank rate measurements with pure AC-HTT-H_2 carbon treated in H_2 at 573 K showed no activity over the temperature range studied.

2.4. DRIFTS studies

To enhance the low signal-to-noise ratio inherent to these carbon-supported catalysts, we diluted them with calcium fluoride and mixed them to give a CaF_2/catalyst ratio of 30/1. Each diluted sample was loaded into the DRIFTS cell and purged with He overnight before it was subjected to an in situ pretreatment. After this reduction step was completed and the sample was cooled to reaction temperature, the first interferrograms was recorded. This was used as the background reference for the fast Fourier transform (FFT) analysis of all subsequent interferrograms recorded for that particular catalyst. We applied the IPA partial pressure by passing 20 cm^3 (STP) min^{-1} UHP He through an IPA saturator held at 279 K, with the use of a cyclohexane (99+%, ACS reagent)/liquid N_2 slush bath [35], and spectra were recorded for each catalyst under the selected reaction conditions. We obtained the spectrum of vapor-phase IPA at 448 K by passing 14 Torr IPA in He over an aluminum mirror placed in the DRIFTS reactor cell. For all DRIFTS samples that were diluted with CaF_2, the measured dehydrogenation rates were the same as those measured for the undiluted samples, and no dehydration activity was seen with the CaF_2-diluted samples [4]. Details of the DRIFTS system and its modifications have been presented previously [36,37].

3. Results

3.1. Adsorption and XRD measurements on monometallic Pt catalysts

The uptakes of H_2 and CO, metal dispersions, and crystallite sizes for the Pt catalysts are listed in Table 2. The analyzed Pt loadings are in parentheses. No dissociative N_2O adsorption was observed on either Pt/C catalyst at 363 K, in contrast to Pt/SiO_2 catalysts [32], and the reason for this is not known at this time. The apparent dispersion of each catalyst was low, but it did increase with reduction temperature. As expected, the H/Pt ratios based on total H_2 uptake were higher than the CO/Pt ratios.

3.2. Adsorption and XRD measurements on Cu–Pt catalysts

A method coupling the dissociative adsorption of N_2O with titration of the resulting adsorbed oxygen by H_2 or CO was used to determine the individual surface concentrations of Cu and Pt and the overall dispersion in these bimetallic Cu–Pt catalysts [34]. The protocol describing the four sequential experiments was outlined previously and is summarized in Table 1, along with the information gathered from each run. The amounts of surface Cu^0, Cu^{1+}, and Pt atoms are compiled in Table 3, and the analyzed metal loadings are again given in parentheses. The results show that as Cu is added to the base Pt catalyst, the total and irreversible uptakes of H_2 and CO decrease, whereas oxygen adsorption via N_2O decomposition at 363 K increases. The total

Table 2
H_2, CO and 'O' chemisorption on, and crystallite size by XRD of, carbon-supported Pt catalysts

Catalyst	T_{RED} (K)	H_2 uptake[a] (μmol g^{-1})	CO uptake[a] (μmol g^{-1})		H_{total}/CO_{irr}	Dispersion		d_{crys} (nm)	
		Total	Total	Irreversible		H_T/Pt_T	CO_{irr}/Pt_T	ads[b]	XRD
1% Pt/AC-HNO_3	473	2.9	10.2	4.0	1.45	0.119	0.082	9.5	4.8
(0.95% Pt)[c]	573	4.8	16.5	8.6	1.12	0.197	0.177	5.7	< 2.5
1% Pt/AC-HTT-H_2	473	4.4	9.6	5.0	1.76	0.177	0.101	6.4	5.2
(0.97% Pt)[c]	573	7.3	16.2	11.4	1.28	0.294	0.229	3.8	4.3
UHP Pt powder	573	3.0	3.8	3.4	1.77	0.0012	0.0007	965	> 100

[a] Values extrapolated to zero pressure.
[b] Based on $d_{crys} = 1.13/(H_T/Pt_T)$.
[c] Analyzed Pt loading.

Table 3
H_2, CO, N_2O chemisorption and titration uptakes on carbon-supported Cu–Pt catalysts

Run	Gas uptake (μmol g^{-1})					H_T/Pt_T	Surface concentration (μmol g^{-1})		
	H_2		CO		'O' uptake[b]		Cu^{+1}	Cu^0	Pt
	Total	Irreversible	Total	Irreversible	Irreversible				
				0.5% Cu-1% Pt/AC-HTT-H_2 (0.50% Cu-0.97% Pt)[a]					
0[c]	8.6	2.5	23.3	16.5	0.0	0.34	0.0	0.0	17.2[d] (16.5)[e]
1	2.3	0.9	–	–	–	–	–	–	4.6
2	–	–	11.3	4.3	–	–	–	–	4.3[f]
3[g]	5.4	3.3	–	–	–	–	–	–	3.6
4[h]	–	–	36.8	29.9	–	–	25.7[i]	–	–
TGA	–	–	–	–	12.9	–	–	17.4[i]	0.0
									4.2 (ave.)
				1% Cu-1% Pt/AC-HTT-H_2 (1.04% Cu-0.97% Pt)[a]					
0[c]	8.6	2.5	23.3	16.5	0.0	0.34	0.0	0.0	17.2[d] (16.5)[e]
1	0.46	0.41	–	–	–	–	–	–	0.92
2	–	–	6.1	2.1	–	–	–	–	2.1[f]
3[g]	0.88	0.69	–	–	–	–	–	–	0.59
4[h]	–	–	25.3	20.0	–	–	18.8[i]	–	–
TGA	–	–	–	–	11.4		–	20.4[i]	0.0
									1.2 (ave.)
				5% Cu-1% Pt/AC-HTT-H_2 (4.96% Cu-0.97% Pt)[a]					
0[c]	8.6	2.5	23.3	16.5	0.0	0.34	0.0	0.0	17.2[d] (16.5)[e]
1	0.27	0.27	–	–	–	–	–	–	0.54
2	–	–	5.7	1.3	–	–	–	–	1.3[f]
3[g]	2.6	2.3	–	–	–	–	–	–	1.7
4[h]	–	–	32.6	28.8	–	–	27.6[i]	–	0.0
TGA	–	–	–	–	15.6	–	–	28.8[i]	0.0
									1.2 (ave.)

[a] Actual analyzed metal loadings.
[b] Determined gravimetrically.
[c] For 1% Pt/AC-HTT-H_2 reduced at 673 K for 1 h.
[d] Based on total H_2 uptake.
[e] Based on irreversible CO uptake.
[f] Assuming no Cu^{+1}.
[g] H_2 titration after N_2O decomposition.
[h] CO titration after N_2O decomposition.
[i] Corrected for Pt_s (ave.).

H_2 uptake on the monometallic 1% Pt/AC-HTT-H_2 catalyst before Cu impregnation was 8.6 μmol g^{-1}. The addition of 0.5% Cu (79 μmol Cu g^{-1}) decreased the uptake to 2.3 μmol H_2 g^{-1}, and the addition of ten times more Cu reduced the total H_2 uptake to 0.3 μmol H_2 g^{-1}, which indicates that Cu is covering the Pt surface and decreasing the number of available surface Pt atoms, Pt_s. The values for total and irreversible CO uptakes behaved similarly with the addition of increasing amounts of Cu, and the decrease in CO uptake that occurred as the Cu content increased suggests that all surface copper atoms are Cu^0, because irreversible CO chemisorption does not occur on Cu^{+2} or Cu^0; therefore, the irreversible CO uptake is due entirely to adsorption on Pt.

Uptakes for total H_2 chemisorption, irreversible CO chemisorption (assuming no Cu^{+1}), and H_2 titration of chemisorbed O atoms from N_2O decomposition should yield the same number of Pt_s atoms if adsorption stoichiometries are $H_T/Pt_s = CO_{irr}/Pt_s = O_{ad}/Pt_s = 1$, no Cu_s^{+1} species are present, and no H spillover occurs from Pt. The agreement is not exact, as can be seen in Table 3, but the numbers are consistent and similar in almost all cases; consequently, average values for the amount of Pt_s in the bimetallic catalysts were used. The 0.5% Cu-1% Pt/AC-HTT-H_2 catalyst had the highest Pt_s concentration (4.2 μmol Pt_s g^{-1}), whereas the other two bimetallic catalysts had ∼ 1 μmol Pt_s g^{-1}. For the bimetallic catalysts there is rather good agreement between the number of Cu^0 surface atoms (Cu_s^0), as determined by dissociative N_2O adsorption on a reduced surface, such as that shown in Fig. 1, and the number of Cu^{1+} surface atoms (Cu_s^{1+}) titrated from an O-covered surface by CO (from isotherms such as those in Fig. 2), after correction for the average number of Pt_s atoms determined from three different subsequent experiments, that is, H_2 chemisorption, CO chemisorption, and H_2 titration of chemisorbed O atoms (Fig. 3). Table 4 summarizes the overall metal dispersion plus the estimated Cu_s and Pt_s surface concentrations in the three bimetallic catalysts.

A typical XRD scan is shown in Fig. 4 for 1% Cu-1% Pt/AC-HTT-H_2. From spectrum C, which has been corrected for the contribution from the support, no Cu peak is observed ($2\theta = 43.29°$), but a Pt(111) reflection at $2\theta = 39.75°$ is identified. A Cu reflection was apparent in the XRD pattern for the 5% Cu-1% Pt samples [31]. The volume-averaged particle sizes calculated from the Scherrer equation are shown in Table 5, as are the surface-averaged particle sizes determined from chemisorption measurements.

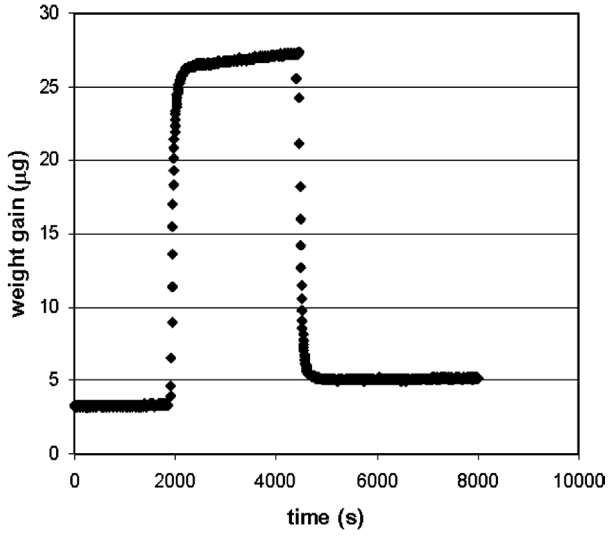

Fig. 1. N_2O decomposition at 363 K on 1% Cu-1% Pt/AC-HTT-H_2 reduced at 573 K.

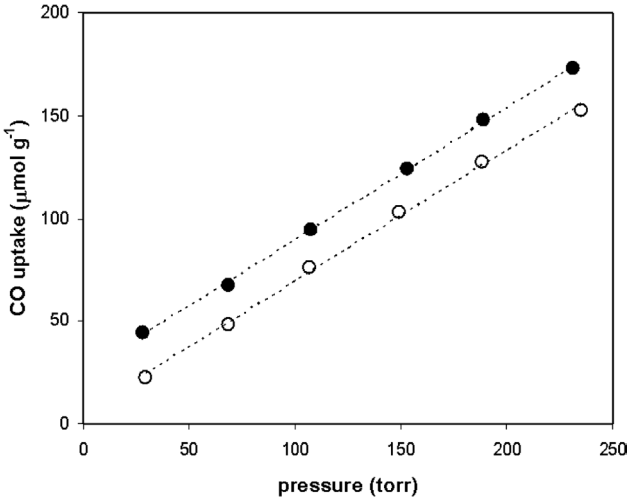

Fig. 2. CO titration at 300 K after N_2O decomposition on 1% Cu-1% Pt/AC-HTT-H_2 reduced at 573 K: total uptake (●), reversible uptake (○).

3.3. XPS, TEM, and TPR characterization of Cu–Pt catalysts

Readily discernible peaks in Fig. 5 for the 1% Cu-1% Pt/AC-HTT-H_2 catalyst are the C (1*s*), O (1*s*), oxygen, and carbon Auger peaks at 285, 531, 745, and 984 eV, respectively [38]. Expansion of the region below 75 eV revealed no detectable lines at 71 and 74 eV for the Pt $4p_{7/2}$ and $4f_{5/2}$ peaks, respectively. The inset of Fig. 5 concentrates on the energy region between 925 and 970 eV, which contains the $2p_{1/2}$ and $2p_{3/2}$ photoelectron lines for Cu at 933 and 953 eV, respectively. The peaks for Cu^0 and Cu^{+1} fall in a narrow energy region of ∼ 932–933 eV, but that for Cu^{2+} falls at a higher binding energy around 934 eV; thus it is evident that no Cu^{2+} is present on the catalyst surface.

With TEM it was difficult to discriminate between Cu and Pt crystallites, so the results shown are a result of count-

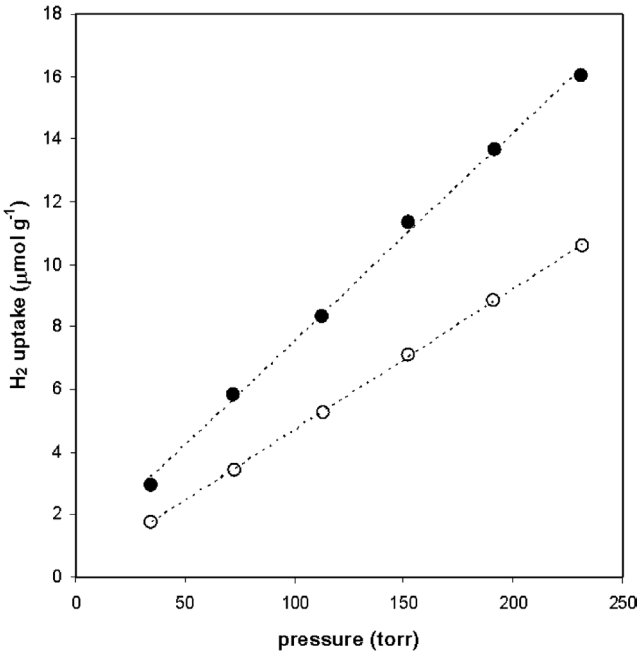

Fig. 3. H_2 titration at 300 K after N_2O decomposition on 1% Cu-1% Pt/AC-HTT-H_2 reduced at 573 K: total uptake (●), reversible uptake (○).

Table 4
Surface composition and total metal dispersion for bimetallic Cu–Pt/AC-HTT-H_2 catalysts

Catalyst	Bulk composition			Surface composition[a] (μmol g^{-1})			Overall dispersion $\left(\frac{Cu_S+Pt_S}{Cu_T+Pt_T}\right)$
	Cu/Pt	(μmol g^{-1})		Cu^0	Pt^0	Cu (%)	
		Cu	Pt				
0.5% Cu-1% Pt/AC-HTT-H_2	1.5/1	79	50	17.4	4.2	81	0.17
1% Cu-1% Pt/AC-HTT-H_2	3/1	164	50	20.4	1.2	94	0.10
5% Cu-1% Pt/AC-HTT-H_2	15/1	780	50	28.8	1.2	96	0.36

[a] No evidence for Cu^{+1} species was obtained for any catalyst.

Table 5
Average Cu–Pt crystallite sizes (nm) from chemisorption, XRD and TEM techniques

Catalyst	Particle size (nm)						
	XRD		Chemisorption		TEM		
	Cu^0 [a]	Pt[b]	Cu^0 [a]	Pt[b]	d_{num}	d_{surf}	d_{vol}
0.5% Cu-1% Pt/AC-HTT-H_2	NOP[c]	15	5.0	13.4	22	30	35
1% Cu-1% Pt/AC-HTT-H_2	NOP[c]	9.5	8.8	46.8	34	41	53
5% Cu-1% Pt/AC-HTT-H_2	9.2	14	29.8	46.8	41	58	68

[a] Based on $d_{surf} = 1.1/(Cu_s^0/Cu_T)$.
[b] Based on $d_{surf} = 1.13/(Pt_s/Pt_T)$.
[c] No observable peak.

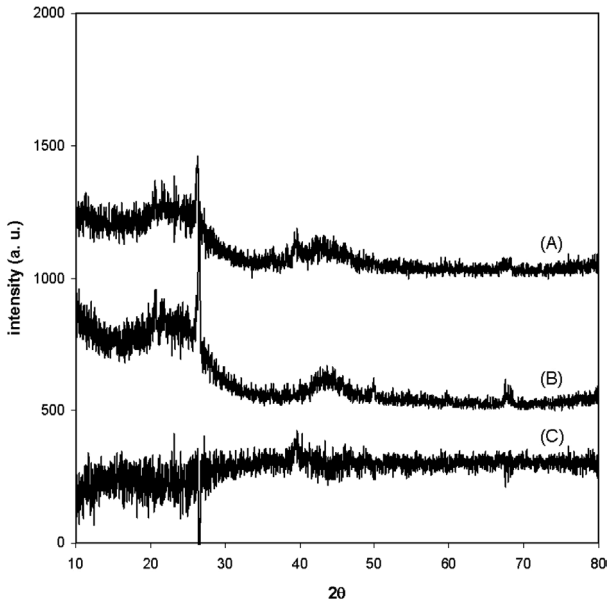

Fig. 4. X-ray diffraction pattern for 1% Cu-1% Pt/AC-HTT-H_2: (A) 1% Cu-1% Pt/AC-HTT-H_2 reduced at 573 K; (B) pure AC-HTT-H_2 reduced at 573 K; (C) after subtraction of (B) from (A).

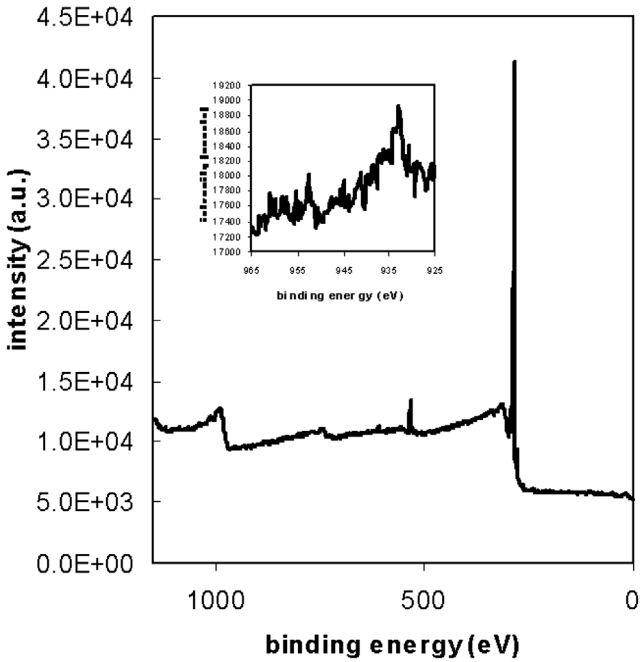

Fig. 5. XPS survey scan of 1% Cu-1% Pt/AC-HTT-H_2 reduced at 573 K. Inset is Cu scan region.

ing both Cu and Pt particles in the bimetallic samples. Two hundred particles were counted for each particle size determination. The number-averaged particle diameter, $d_{num} = \Sigma n_i d_i / \Sigma n_i$, was 22, 34, and 41 nm for the 0.5, 1, and 5% Cu-1% Pt/AC-HTT-H_2 catalysts, respectively; TEM micrographs are provided elsewhere [31].

Temperature-programmed reduction results are shown in Fig. 6. Maximum reduction rates for monometallic Cu and Pt catalysts were around 560 and 440 K, respectively. The peak for H_2 consumption with Cu/AC-HTT-H_2 was very broad, suggesting that either Cu particles are supported on an energetically heterogeneous surface or the reduction of copper is occurring through a stepwise mechanism ($Cu^{+2} \rightarrow Cu^{+1} \rightarrow Cu^0$), as well as directly from CuO to Cu^0. As Cu was added to the 1% Pt/AC-HTT-H_2 catalyst, the Pt reduction peak decreased from ∼ 440 to 430 K, regardless of the Cu amount. The TPR spectra for the bimetallic samples show that Cu began to reduce at lower temperatures, presumably because of H spillover, but over a very broad temperature range, and only the 5% Cu-1% Pt/AC-HTT-H_2 catalyst had a Cu reduction peak. These results are consistent with the Pt-catalyzed

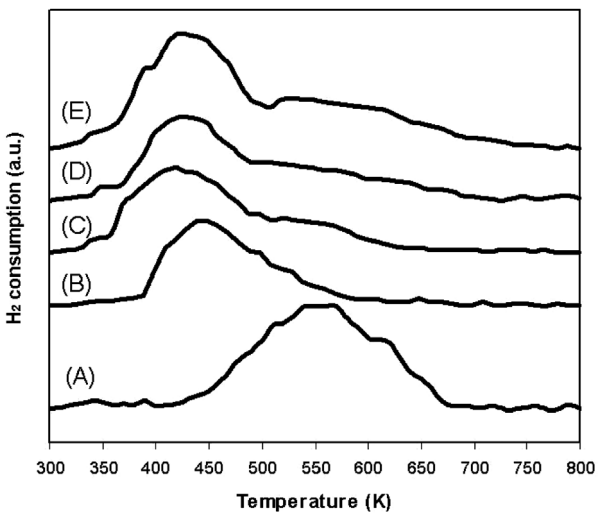

Fig. 6. Temperature programmed reduction of: (A) 1% Cu/AC-HTT-H_2, (B) 1% Pt/AC-HTT-H_2, (C) 0.5% Cu-1% Pt/AC-HTT-H_2, (D) 1% Cu-1% Pt/AC-HTT-H_2 and (E) 5% Cu-1% Pt/AC-HTT-H_2.

Table 6
IPA dehydrogenation on Pt/C catalysts (reaction conditions: $P_{IPA} = 14$ Torr, $T = 448$ K)

Catalyst	T_{RED} (K)	Dispersion (H_T/Pt_T)	Activity[a] ($\mu mol\ g^{-1}\ s^{-1}$)	TOF[b] (s^{-1})	E_a ($kcal\ mol^{-1}$)	Selectivity (%)	
						Acetone	Propylene
1% Pt/AC-HNO_3	473	0.119	1.0	0.17	5.0	90	10
	573	0.197	1.5	0.16	9.4	100	0
1% Pt/AC-HTT-H_2	473	0.177	1.1	0.13	7.3	100	0
	573	0.294	1.6	0.11	6.8	100	0
UHP Pt powder	573	0.0012	0.066 (0.11)[c]	0.011 (0.018)[c]	9.1 (11.6)[c]	98	2[d]

[a] Disappearance of IPA measured at 14 Torr IPA and 448 K.
[b] Based on total H_2 chemisorption.
[c] Disappearance of IPA measured at 14 Torr IPA, 30 Torr H_2 and 448 K.
[d] Based on retention time, product is most likely propane, not propylene.

reduction of CuO [39]. These TPR results imply that Pt and Cu are in intimate contact, and only after the addition of 5% Cu to the base Pt catalyst does a significant fraction of the Cu behave like Cu in the monometallic catalyst.

3.4. Kinetics of IPA dehydrogenation on monometallic Pt catalysts

The dehydrogenation of IPA was studied over Pt dispersed on an activated carbon that had been prepared to give two different surfaces, that is, one with acidic O-containing functional groups (AC-HNO_3) and one that was hydrophobic after a high-temperature treatment at 1223 K in H_2 (AC-HTT-H_2). An ultra-high-purity Pt powder was also used for kinetic studies. Pt was considerably more active than Cu for IPA dehydrogenation, on both a gram catalyst and a TOF basis [4,31]. Steady-state activities, TOFs (based on H_2 chemisorption results), and apparent activation energies for the Pt catalysts after different pretreatments are listed in Table 6. A Pt/AC-ASIS catalyst (activated carbon with no treatment) was not prepared because a Cu/AC-ASIS catalyst used in a previous study had a very low activity, compared with either Cu/AC-HNO_3 or Cu/AC-HTT-H_2 [4,31]. This was attributed to an impurity in the carbon that was either removed or altered by the HNO_3 or the HTT-H_2 treatment. Unlike the activities of the Cu catalysts, the activities of the Pt/AC-HNO_3 and Pt/AC-HTT-H_2 catalysts were comparable, and the selectivity for propylene (from the dehydration reaction due to the acidic sites on the C surface) was lower on Pt/AC-HNO_3 compared with Cu/AC-HNO_3. In fact, for a sample of 1% Pt/AC-HNO_3 reduced at 573 K, there was no detectable production of propylene. The TOFs for the Pt/C catalysts varied only from 0.11 to 0.17 s^{-1}, and the Pt/AC-HNO_3 catalysts had a slightly higher value than the Pt/AC-HTT-H_2 catalysts, which is the opposite of the observation for Cu catalysts. The carbon-supported catalysts were active and extremely stable with time on stream [31], whereas the Pt powder deactivated significantly; consequently, the "steady-state" TOF for Pt powder with either 0 or 30 Torr H_2 in the feed was only 0.011 or 0.018 s^{-1}, respectively. This deactivation was caused by the formation of a carbonaceous species on the Pt surface, and the powder could be regenerated by heating in H_2 at 473 or 573 K [31]. These catalysts were 100% selective for acetone, except for 1% Pt/AC-HNO_3 reduced at 473 K, which gave 10% propylene, and the Pt powder, which gave what appeared to be 2% propane [31]. Addition of hydrogen to the feed had no effect on selectivity for this latter, unidentified product. Apparent activation energies for IPA dehydrogenation over the various Pt catalysts obtained from the Arrhenius plots are shown in Fig. 7.

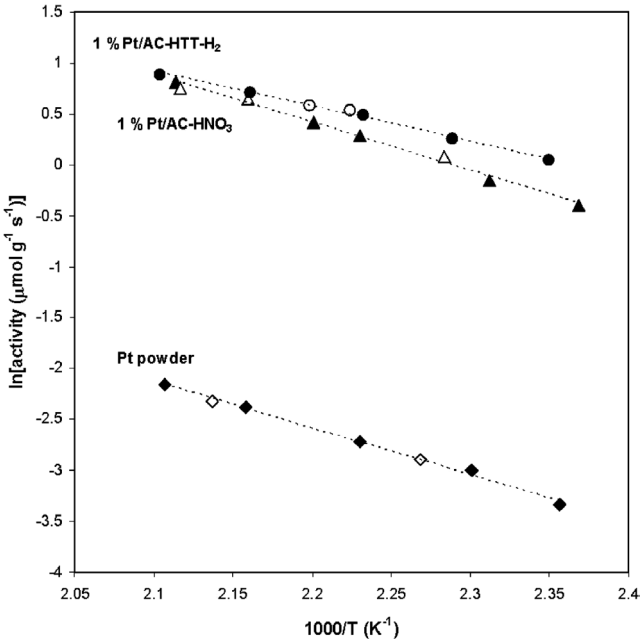

Fig. 7. Arrhenius plots for Pt catalysts reduced at 573 K; reaction conditions were 14 Torr isopropanol and 423–473 K.

The Weisz–Prater (W-P) criterion [40] was used to check for the absence of any significant transport limitations in each of the catalysts, and the necessary physical parameters of the carbon were obtained from a study by Ma [41]. For all catalysts, the values of the dimensionless W-P parameter were orders of magnitude below 0.3, thus verifying that the kinetic data obtained in this study were free of mass transport effects.

Table 7
Reaction orders for IPA dehydrogenation on Pt/C catalysts

Catalyst	T_{RXN}	Reaction order		
		Isopropanol	H_2	Acetone
1% Pt/AC-HTT-H_2	433	0.34	−0.06	−0.05
	448	0.37	−0.04	−0.04
	458	0.45	−0.03	−0.01
	473	0.53	−0.03	0

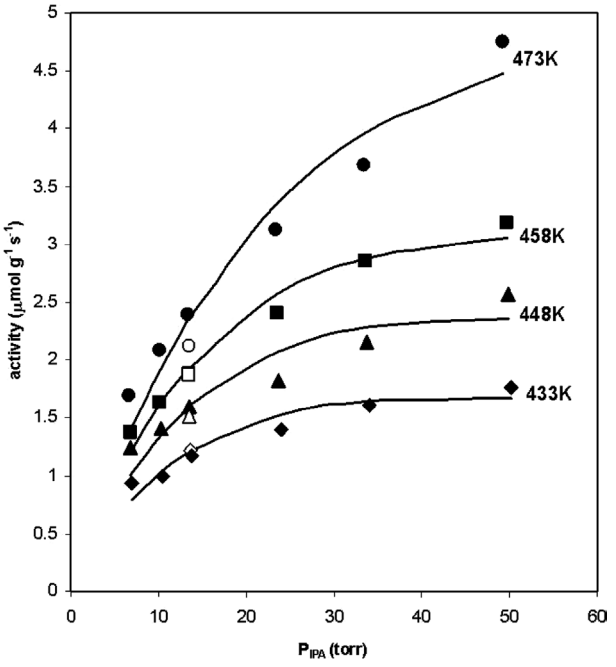

Fig. 8. Isopropanol partial pressure data for 1% Pt/AC-HTT-H_2 reduced at 573 K; symbols, experimental data; lines, predicted rates.

Partial pressure dependencies on IPA and the two reaction products, H_2 and acetone, at four different temperatures are compiled in Table 7 and shown in Figs. 8–10. Similar to the Cu catalysts [4], the dependence on IPA approached unity with increasing temperature, whereas H_2 and acetone yielded slightly negative to zero-order dependencies.

3.5. Kinetics of IPA dehydrogenation on bimetallic Cu–Pt catalysts

Like their monometallic Pt or Cu [4] counterparts, all bimetallic catalysts with the AC-HTT-H_2 support were 100% selective for acetone, the dehydrogenation product. After reduction at 573 K, the pure AC-HTT-H_2 support had no detectable activity [4,31]. Whereas selectivity was not affected by the bimetallic composition, there was significant variability in the reaction rate among the monometallic and bimetallic catalysts, expressed either as activity or as a TOF. Activity maintenance profiles for the three bimetallic catalysts are shown in Fig. 11. The TOF at 448 K on the monometallic Cu or the Pt/AC-HTT-H_2 catalyst was 2×10^{-2} s^{-1} or 11×10^{-2} s^{-1}, respectively, whereas TOFs measured for the three bimetallic catalysts were similar to

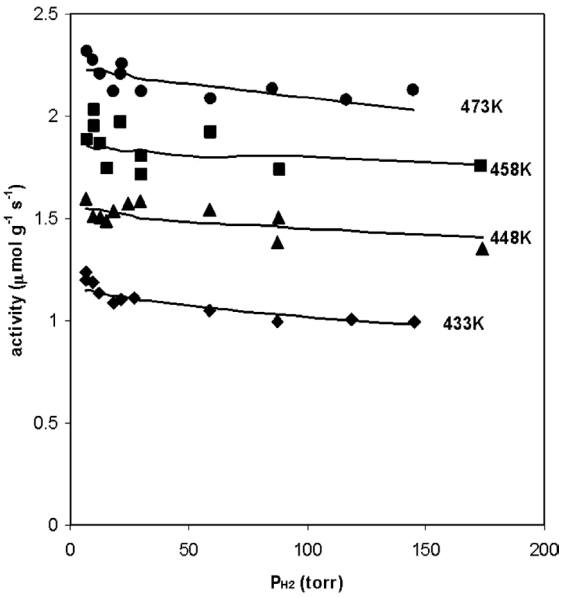

Fig. 9. H_2 partial pressure data for 1% Pt/AC-HTT-H_2 reduced at 573 K; symbols, experimental data; lines, predicted rates.

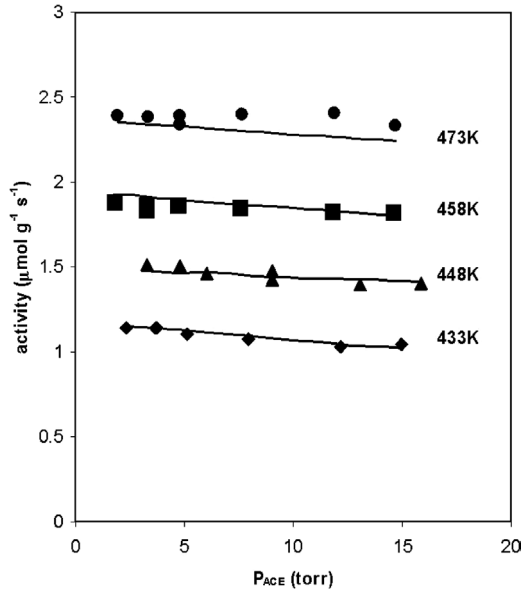

Fig. 10. Acetone partial pressure data for 1% Pt/AC-HTT-H_2 reduced at 573 K; symbols, experimental data; lines, predicted rates.

or noticeably lower than that for the Cu/C catalyst, as they ranged from 0.6×10^{-2} to 4×10^{-2} s^{-1}. Steady-state activities behaved in a similar fashion and are listed in Table 8.

Activation energies for the bimetallic catalysts were measured over a wider temperature range than the monometallic catalysts. The apparent activation energy for the two catalysts with the lowest Cu loading changed at higher temperatures, and for 0.5% Cu-1% Pt/AC-HTT-H_2 the activation energy decreased from 7.2 to 4.4 kcal mol^{-1} as the temperature increased, whereas with 1% Cu-1% Pt/AC-HTT-H_2, it decreased from 9.2 to 2.4 kcal mol^{-1} as the temperature increased. The Arrhenius plots for either catalyst exhibited

Table 8
IPA dehydrogenation on Cu, Pt and Cu–Pt/C catalysts (reaction conditions: $P_{IPA} = 14$ Torr, $T = 448$ K)

Catalyst	Surface composition (μmol g^{-1})		$Cu_s/(Cu_s + Pt_s)$	E_a (kcal mol^{-1})	Activity[a,b] (μmol g^{-1} s^{-1})	TOF[a,c] (s^{-1})
	Cu_s	Pt_s				
1% Pt/AC-HTT-H_2	0	14.6	0	6.8	1.60	0.11
0.5% Cu-1% Pt/AC-HTT-H_2	17.4	4.2	0.81	7.2/4.4[d]	0.92	0.043
1% Cu-1% Pt/AC-HTT-H_2	20.4	1.2	0.94	9.2/2.4[d]	0.23	0.011
5% Cu-1% Pt/AC-HTT-H_2	28.8	1.2	0.96	9.0	0.18	0.006
1% Cu/AC-HTT-H_2[e]	17.8	0	1	20.5	0.38	0.021
5% Cu/AC-HTT-H_2[e]	135	0	1	21.4	2.70	0.020

[a] Reaction conditions were 14 Torr IPA and 448 K.
[b] Average of five runs with five different samples.
[c] Based on total number of metal (Cu and Pt) surface atoms.
[d] Low-T region/high-T region. See text for details.
[e] Taken from Ref. [4].

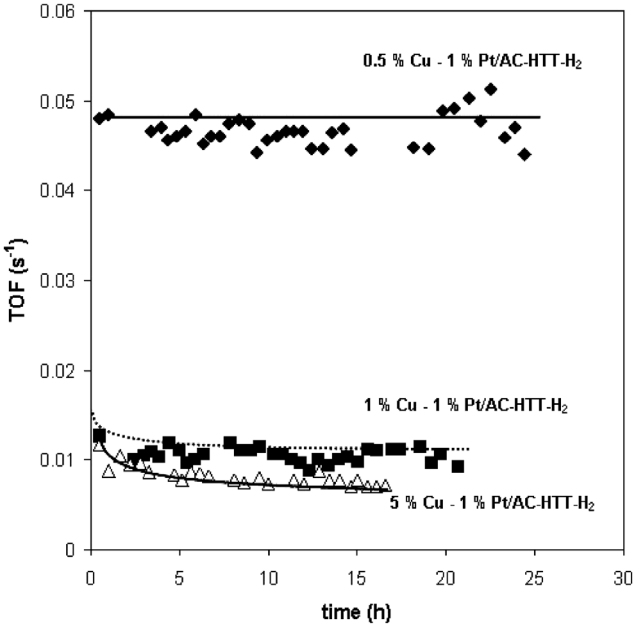

Fig. 11. Activity maintenance of Cu–Pt/HTT-H_2 catalysts after reduction at 573 K: reaction conditions were 14 Torr isopropanol and 448 K, and activity is normalized to total surface Cu plus Pt atoms.

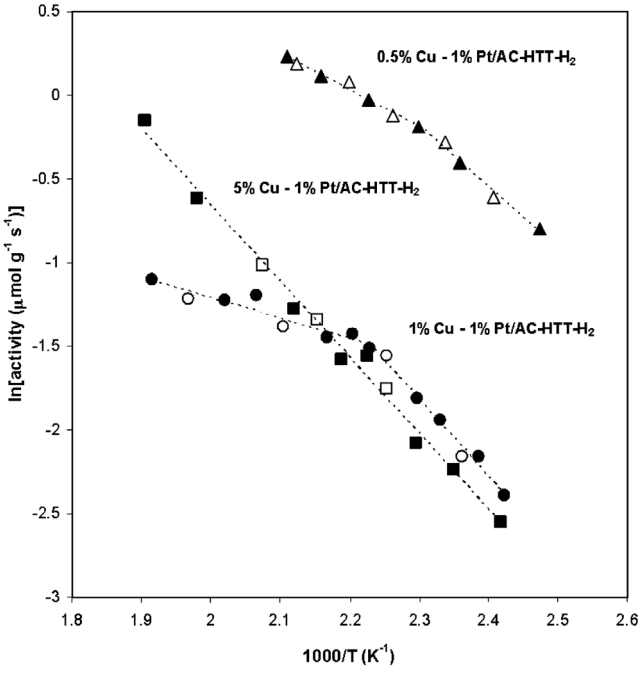

Fig. 12. Arrhenius plots for Cu–Pt catalysts reduced at 573 K: reaction conditions were 14 Torr isopropanol and 413–523 K.

bend-over behavior around 443 K. The least active 5% Cu-1% Pt/AC-HTT-H_2 catalyst had an apparent activation energy of 9.0 kcal mol^{-1} between 413 and 523 K, compared with 20.5 kcal mol^{-1} with the 5% Cu/AC-HTT-H_2 catalyst. Arrhenius plots for the three bimetallic catalysts are shown in Fig. 12.

The activation energy of around 7–9 kcal mol^{-1} for the bimetallic catalysts in the low-temperature (403–443 K) region was similar to that for Pt. As the temperature increased above 448 K, the influence of copper was apparent, but inconsistent with monometallic Cu behavior, because at higher temperatures the higher E_{app} value for Cu/C should enhance the activity and allow it to surpass that of the Pt component. In contrast, in the high-temperature regime between 448 and 523 K, no increase in the apparent activation energy occurred, and, in fact, E_{app} decreased to only 2–4 kcal mol^{-1} for the two Cu–Pt catalysts with the lowest Cu content. Such a trend in apparent activation energy can suggest pore diffusion control, so the Weisz–Prater (W-P) criterion was used to determine whether these kinetic data were affected by mass transfer limitations. The calculated dimensionless W-P parameters were orders of magnitude lower than 0.3, indicating that no significant pore diffusional effects existed [31]. Heat transfer limitations were considered to be unimportant because of the mild endothermicity of the reaction and differential reactor operation. Therefore, the decrease in activation energy is not attributed to mass transfer limitations, but to some factor in the kinetics of the reaction, such as a shift in the RDS or a large change in the surface coverage of one of the components in the system, as discussed later.

To facilitate kinetic modeling, partial pressure dependencies were determined over a temperature range of 70 K for

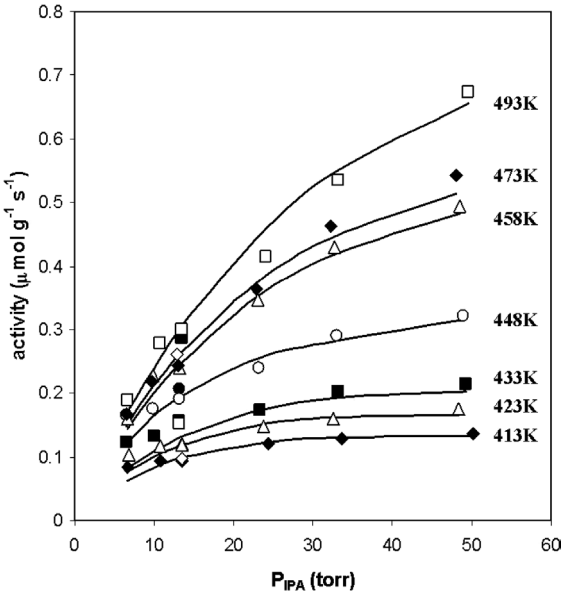

Fig. 13. Isopropanol partial pressure data for 1% Cu-1% Pt/AC-HTT-H_2 reduced at 573 K; symbols, experimental data; lines, predicted rates.

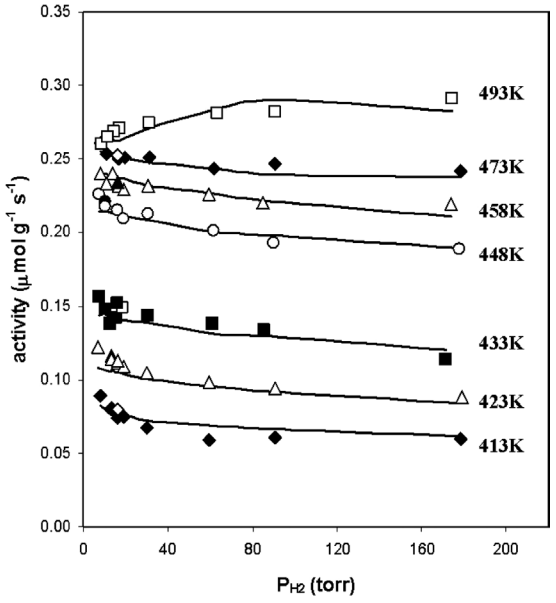

Fig. 14. H_2 partial pressure data for 1% Cu-1% Pt-AC-HTT-H_2 reduced at 573 K; symbols, experimental data; lines, predicted rates.

all three bimetallic catalysts with AC-HTT-H_2 as a support, and the activity dependencies on partial pressure are shown in Figs. 13–15 for 1% Cu-1% Pt as a typical example. Comparable results were obtained for the other two bimetallic catalysts, and they are shown elsewhere [31]. The power-rate law reaction orders for IPA, hydrogen, and acetone obtained from these figures are compiled in Table 9. Similar to the monometallic Pt catalyst, hydrogen and acetone had small negative dependencies, and the magnitude of this dependency was independent of bimetallic composition. The partial-pressure dependency on IPA for the three bimetallic catalysts was influenced by the amount of surface copper

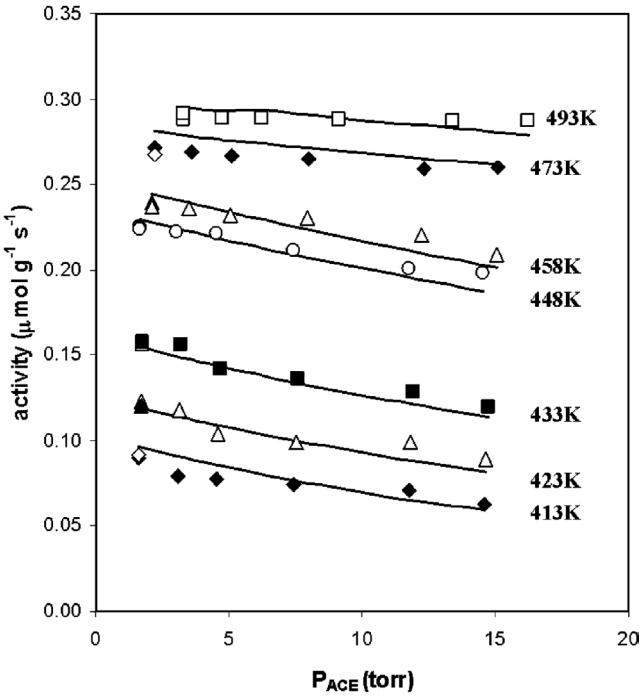

Fig. 15. H_2 partial pressure data for 1% Cu-1% Pt/AC-HTT-H_2 reduced at 573 K; symbols, experimental data; lines, predicted rates.

Table 9
Reaction orders for IPA dehydrogenation on carbon-supported Cu–Pt catalysts

Catalyst	T_{RXN}	Reaction order		
		Isopropanol	H_2	Acetone
0.5% Cu-1% Pt/AC-HT-H_2	413	0.15	−0.17	−0.13
	423	0.18	−0.15	−0.10
	433	0.22	−0.13	−0.07
	448	0.34	−0.07	−0.04
	458	0.37	−0.03	−0.03
	473	0.48	−0.02	−0.02
	493	0.54	0.01	0
1% Cu-1% Pt/AC-HTT-H_2	413	0.27	−0.13	−0.14
	423	0.28	−0.10	−0.13
	433	0.30	−0.07	−0.11
	448	0.37	−0.05	−0.08
	458	0.58	−0.03	−0.03
	473	0.61	−0.02	−0.01
	493	0.64	0.03	0
5% Cu-1% Pt/AC-HTT-H_2	433	0.03	−0.17	−0.12
	448	0.07	−0.13	−0.09
	458	0.12	−0.04	−0.07
	473	0.32	−0.03	−0.02

present. For the bimetallic catalyst with the highest Cu loading, the dependence on the IPA pressure was similar to that for the monometallic Cu catalyst [4], but for the two bimetallic samples with lower Cu loadings, the reaction order on IPA was similar to that for Pt (see Table 7).

A DRIFT spectrum of 0.5% Cu-1% Pt/AC-HTT-H_2 under reaction conditions (14 Torr IPA and 448 K) after reduction at 573 K is shown in Fig. 16, in which the vapor-phase spec-

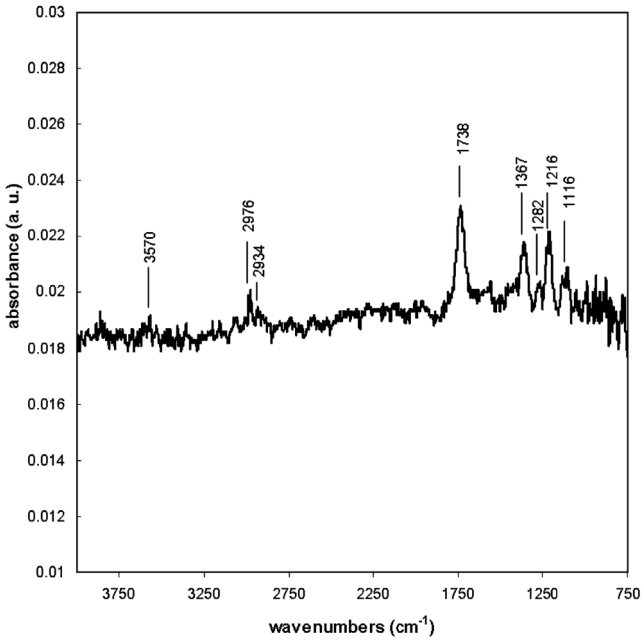

Fig. 16. DRIFT spectrum of 0.5% Cu-1% Pt/AC-HTT-H_2 reduced at 573 K under reaction conditions (14 Torr isopropanol and 448 K). Gas-phase isopropanol and acetone have been subtracted.

tra for IPA and acetone have been subtracted. Comparable spectra with the pure AC-HTT-H_2 carbon showed indistinct bands barely above the noise level at 400 K, and no bands were visible at 460 K. The spectrum for the monometallic Pt catalyst, shown elsewhere [31], is similar to that in Fig. 16, and both differ from the spectrum obtained with the 1% Cu/AC-HTT-H_2 catalyst [4]. In Fig. 16, the most prominent band near 1740 cm^{-1}, which was absent from the monometallic copper spectrum, is evidence for adsorbed acetone, assigned to the carbonyl stretching mode in acetone. The bands at 1367, 1216, and 1116 cm^{-1} can also be attributed to acetone, as they are in good agreement with results from Cu/carbon films [16]. These bands are associated with CH_3 symmetric deformation (1364 cm^{-1}), a CC stretch (1216 cm^{-1}), and a CH_3 rocking mode (1090 cm^{-1}); the wavenumbers in parentheses are vapor-phase values [42]. It should be noted that it can be difficult to discern between surface isopropoxide species and molecularly adsorbed isopropanol without the aid of additional characterization techniques [10]. Previous results for a 1% Cu/AC-HTT-H_2 catalyst strongly suggested the presence of an adsorbed isopropoxide species, but adsorbed molecular IPA could not be excluded, and therefore both were included in a site balance [4]. Vibrational spectra provided evidence for adsorbed molecular IPA on the surface of both monometallic Pt and bimetallic Cu–Pt catalysts. For both catalysts, bands near 1285, 2930, 2976, and 3545 cm^{-1} are characteristic vibrations of molecular IPA. The presence of an isopropoxide species on the catalyst surface cannot be completely ruled out, but there is no direct evidence for its existence from these infrared spectra.

4. Discussion

4.1. Characterization

A thorough characterization of carbon supports similar to those used in this study, by TPD, XRD, and DRIFTS, has been published [30]. The dispersion of metal crystallites on carbon is of interest because of the widespread use of such systems in heterogeneous catalysis, and it is known that the allotropic form of carbon can influence the dispersion of a metal species [43,44]. The surface chemistry of these carbons can be modified by various pretreatments [30], such as a high-temperature heat treatment (HTT) or washing with acidic or basic solutions, which can have a significant effect on metal dispersion. The influence of carbon surface chemistry on the dispersion of Cu [45] and Pt [46–59] has been investigated. In the present study, the type of pretreatment of this activated carbon had a smaller effect on Pt dispersion than that recently reported for Cu [43]; however, after a particular reduction temperature Pt had a consistently higher apparent dispersion on the AC-HTT-H_2 carbon. One problem associated with the use of carbon as a support is the frequent inability to achieve satisfactory batch-to-batch reproducibility [60], which may be due to the significant amount and variety of impurities present. A significant amount of Na (1200 ppm) was detected in this carbon, and alkali metals such as Na and K can cover a fraction of the Pt surface and decrease H_2 adsorption capability [61,62]. If one pretreatment technique was more efficient at removing or deactivating this Na, a higher apparent Pt dispersion could result. It is also possible that the increase in available surface area may have enhanced the Pt dispersion because the HTT step increased the apparent surface area to 1137 $m^2\,g^{-1}$, whereas the HNO_3 step added surface functional groups and decreased the surface area to 616 $m^2\,g^{-1}$. The more hydrophilic nature of the HNO_3-treated carbon did not result in a higher Pt dispersion, in contrast to other systems using aqueous impregnation [49,63].

A combination of selective chemisorption plus titration methods after dissociative N_2O adsorption at 363 K provided characterization of the surface of these bimetallic Cu–Pt crystallites [31,34]. These methods were initially applied to silica-supported Cu and Pt catalysts, and they have been extended here to the carbon-supported metals. Based on these studies and those on supported Cu systems [45,64] and Pt catalysts [61,65], the following surface processes are applicable to defining the bimetallic surfaces:

$$2Cu_s + N_2O_{(g)} \xrightarrow{363\ K} Cu_s\!\!<\!\!\overset{O}{}\!\!>\!\!Cu_s + N_{2(g)}, \tag{1}$$

$$Cu_s\!\!<\!\!\overset{O}{}\!\!>\!\!Cu_s + 2CO_{(g)} \xrightarrow{300\ K} OC\!-\!Cu_s\!\!<\!\!\overset{O}{}\!\!>\!\!Cu_s\!-\!CO, \tag{2}$$

$$2Pt_s + H_2 \xrightarrow{300\ K} 2Pt_s\text{–}H, \tag{3}$$

$$Pt_s + CO \xrightarrow{300\ K} Pt_s\text{–}CO, \tag{4}$$

$$Pt_s + N_2O \xrightarrow{363\ K} Pt_s\text{–}O + N_{2(g)}, \quad (5)$$

$$Pt_s\text{–}O + 2CO_{(g)} \xrightarrow{300\ K} Pt_s\text{–}CO + CO_{2(g)}, \quad \text{and} \quad (6)$$

$$Pt_s\text{–}O + \tfrac{3}{2}H_{2(g)} \xrightarrow{300\ K} Pt_s\text{–}H + H_2O_{(ad)}. \quad (7)$$

No equation is written for H_2 chemisorption on Cu because near 300 K the coverage of both reversibly and irreversibly adsorbed H atoms is far below monolayer coverage, and no precise adsorption stoichiometry exists [66].

It has been shown previously that a reduction temperature of 573 K is sufficient for the total reduction of CuO to Cu^0 on a HTT-H_2 carbon and that no irreversible CO adsorption occurs on Cu^0 or Cu^{+2} sites [4,45,64]. Consequently, Eqs. (1)–(7) can be used to estimate the total metal dispersion and the individual amounts of Cu^0 and Pt on the surface of these metal particles if it is assumed that (1) no Cu^{1+} species are present after reduction, (2) the H_2 titration reaction at 300 K involves only Pt_s–O sites, and (3) irreversible CO adsorption occurs only on Pt_s sites in a reduced catalyst. If it is further assumed that H adsorption on the Cu atoms is negligible or low near 300 K, as indicated by a previous study [66], then the total H_2 adsorption provides another independent estimate for Pt_s. If all of these assumptions are valid and Eqs. (1)–(7) represent reasonably accurate adsorption stoichiometries, then the Pt_s values based on H_{ad}, CO_{ad}, and H_2-N_2O titration should be approximately the same and the Cu^0 and Cu^{1+} values should be equal, provided no sintering occurs. These conditions are reasonably well satisfied, as indicated in Table 3; the greatest discrepancy is the Cu_s concentration in the 0.5% Cu-1% Pt catalyst. Based on average values of these results, overall metal dispersions and surface compositions were estimated; these are listed in Table 4. A distinct interaction occurs between the Cu and Pt atoms, as expected from previous studies [67–71], and most of the Pt surface is covered by Cu atoms.

Copper can exist in a cupric (Cu^{2+}), a cuprous (Cu^{1+}), or a metallic (Cu^0) state, and the distribution of these oxidation states can depend upon both reduction temperature and the support pretreatment used [45]. This previous study also indicated that Cu reducibility is dependent on crystallite size because 6–8-nm Cu crystallites on AC-HTT-H_2 were much more easily reduced than 25–35-nm Cu crystallites on AC-HNO_3 [4]. Robertson et al. have found that Cu dispersed on SiO_2 is easier to reduce than unsupported CuO, which may also be attributable to a particle size effect [72]. Baker and co-workers have shown that reduction to Cu^0 is dependent upon the Cu precursor and the weight loading of Cu, and two reduction peaks at about 503 and 613 K are attributable to the stepwise reduction of Cu^{2+}, first to Cu^{1+}, then to Cu^0 [43,44]. The H_2 consumption peak maximum at 570 K obtained with the monometallic 1% Cu/AC-HTT-H_2 catalyst (Fig. 6A) is consistent with the 613 K peak reported by Baker and co-workers.

The TPR profiles of a number of Pt precursor salts demonstrate that the temperature of maximum hydrogen consumption is dependent upon the Pt salt [39], and reduction of pure chloroplatinic acid (H_2PtCl_6), which was used in the present study, had a maximum H_2 consumption peak near 400 K. This is consistent with the maximum observed in Fig. 6 for the Pt-containing catalysts. The presence of the Pt clearly facilitates the reduction of the Cu salt, undoubtedly because of H spillover [39,73,74], and no evidence was obtained by any technique—chemisorption, XRD, or XPS—indicating the presence of any Cu oxidation state other than Cu^0.

4.2. Kinetic behavior

Carbon-supported Pt catalysts are much more active for IPA dehydrogenation than their Cu counterparts, and on a TOF basis, Pt is 5 times more active than Cu. Pt is known to be more active for hydrogenation/dehydrogenation reactions than Cu [75], although Cu has better selectivity in dehydrogenation reactions [76,77]. The dehydrogenation of IPA on a Pt/Al_2O_3 catalyst is structure-insensitive [6], and Echevin and Teichner have convincingly shown that the dehydrogenation of butan-2-ol is also a structure-insensitive reaction on Cu/Al_2O_3, because 18 Cu catalysts with dispersions ranging from 0.07 to 0.7 gave the same TOF of $2.7 \times 10^{-3}\ s^{-1}$ at 451 K [78]. Djéga-Mariadassou et al. measured the TOF for IPA dehydrogenation on various crystal planes of zinc oxide and determined that the reaction is structure-insensitive, with TOFs similar to those reported by Echevin and Teichner [79]. Definitive conclusions about structure sensitivity could not be reached in our earlier study of Cu because of the narrow range of metal dispersion. The TOF on the Pt powder (particle size = 965 nm) was an order of magnitude lower than that on the 1% Pt/AC-HTT-H_2 catalyst reduced at 573 K (Pt particle size = 3.8 nm). However, the Pt powder exhibited significant deactivation with time on stream, thus complicating a good comparison.

The power rate laws differed among the catalysts, and the pressure dependence on IPA was greater for Pt than for Cu. The products had slightly less influence during the Pt-catalyzed dehydrogenation reaction, which was reflected in the tendency for reaction orders on products to be closer to zero with Pt compared with Cu. This is interesting because DRIFT spectra of 1% Pt/AC-HTT-H_2 [31] indicated the presence of adsorbed acetone under reaction conditions, whereas there was no indication of adsorbed acetone in a DRIFT spectrum of Cu/AC-HTT-H_2 [4]. This may be related to the relatively low conversion ($\sim$ 1%) in the DRIFTS cell with the monometallic copper sample [31]. With the monometallic Pt catalyst, the conversion in the DRIFTS cell was $\sim$ 3%, thus providing a higher concentration of acetone in the diluted catalyst bed. Subsequently the kinetic data for 1% Pt/AC-HTT-H_2 can be fit by the same Langmuir–Hinshelwood model previously proposed for a 1% Cu/AC-HTT-H_2 catalyst [4].

The addition of Cu to the 1% Pt/AC-HTT-H_2 catalyst had a significant effect not only on activity, but also on kinetic

parameters such as the apparent activation energy, which changed with temperature. As discussed earlier, chemisorption results showed that the addition of Cu to the base Pt catalyst reduced the H_2 chemisorption capacity of the original monometallic Pt catalyst, suggesting that Cu was covering the Pt. A bimetallic Cu–Pt catalyst might be expected to behave more like Pt at low Cu loadings and more like Cu at higher Cu loadings if the metals behave independently of each other. The addition of only 0.5% Cu to 1% Pt/AC-HTT-H_2 decreased the TOF by a factor of about 2.5, and a comparison of the TOFs in Table 8 indicates that the addition of more Cu (up to 5 wt%) decreased the TOF by a factor of up to 18, and it surprisingly became less than that for Cu alone. The higher TOF with the monometallic Cu catalyst may be related to a higher coverage of IPA. A study by Sinfelt and co-workers of a Cu–Ni catalyst for the dehydrogenation of cyclohexane showed that the specific activity of nickel for this reaction changed little over a wide range of Cu–Ni compositions and actually increased somewhat upon the addition of the first increments of copper [80,81]. Only when the catalyst composition approached pure copper was a marked decline in catalytic activity observed, and it was postulated that the RDS changes as the catalyst converts from a Ni-rich to a Cu-rich composition.

Very few studies have examined the behavior of bimetallic catalysts for IPA dehydrogenation. It has been reported that the rate of IPA dehydrogenation in the vapor phase at 363 K was higher on a Ru–Pd/C catalyst than on a Ni catalyst [82,83], but neither paper reported TOFs, so a direct comparison between the two catalysts cannot be made. In a more thorough investigation, Ando et al. found that the rate of IPA dehydrogenation was enhanced on carbon-supported Ru–Rh and Ru–Pt catalysts when compared with the three monometallic catalysts, and kinetic isotope studies indicated that dissociation of the α-H bond was the RDS on monometallic Pt/C and Rh/C catalysts, whereas H_2 desorption appeared to be the slow step on the Ru/C catalyst [84]. It was anticipated that Pt and Rh would act as a hydrogen sink and the surface Ru atoms would break the α-H bond, which was the RDS on both Rh and Pt. Initial rates on the bimetallic catalysts increased by as much as 64% on a gram catalyst basis, but unfortunately no data were provided for the calculation of TOFs. Based on these rates, the activity of these catalysts increased as follows: Ru–Rh > Ru–Pt > Ru > Rh ≫ Pt [84]. The higher activity of the Ru–Rh and Ru–Pt catalysts was attributed to a synergistic effect between the two metals, leading to an enhanced H removal pathway from Ru to Pt or Rh atoms via a spillover mechanism to increase the rate of H atom removal from the Ru surface atoms. In a systematic study of the effect of Ru/Pt atomic ratios between 0 and 4, Ito et al. found that the rate of IPA dehydrogenation at 363 K in the liquid phase was highest on a Ru–Pt/C catalyst with a Ru/Pt ratio of 1 [85]. Rates (per gram) versus composition gave a volcano plot as monometallic Ru/C and Pt/C had comparable activities, and physically mixed systems gave no rate enhancement. Ito et al. also found that the value of the acetone equilibrium adsorption constant in the rate expression decreased as the Pt content increased [85]. The activity and TOF of the Cu–Pt catalysts examined in this study were not enhanced compared with those of the monometallic catalysts, unlike in earlier studies, which may be due in part to both Cu and Pt having the same RDS. However, the binding energy of H atoms on Pt or Cu is lower than that on Ru [86], and because H_2 desorption does not appear to be the RDS, the synergistic effect observed with Ru might not be anticipated. It has been proposed that an electronic effect could occur in a bimetallic system such as a Cu–Pt catalyst to decrease the activity in a reaction like IPA dehydrogenation [1,2]. This may explain the observed behavior.

A Langmuir–Hinshelwood model was proposed for IPA dehydrogenation on carbon-supported copper catalysts, which not only fit the experimental data well, but also yielded thermodynamic parameters that were physically meaningful [4]. The same reaction model was applied to the Pt/C and Cu–Pt/C catalysts studied here; that is, rupture of the O–H bond in an adsorbed IPA molecule to form a surface isopropoxide species was chosen as the RDS. Quasi-equilibrium was proposed to exist between gas-phase IPA, acetone, and H_2 and their adsorbed counterparts (assuming H atoms). The formation of a hydrogen molecule from IPA was assumed to occur via the removal of a H atom in two sequential elementary steps on the catalyst surface; consequently, two Langmuir–Hinshelwood rate expressions were derived and examined—one based on removal of the first H atom as the RDS and the other based on removal of the second H atom as the RDS [31]. In either case, the first hydrogen atom removed is most likely the hydroxyl hydrogen, even though the O–H bond is somewhat stronger than the C–H bonds [87,88], and the adsorbed intermediate formed is an isopropoxide species. As with the Cu/C catalysts, the former model was better; hence, the series of elementary steps for the overall dehydrogenation reaction are

$$(CH_3)_2CHOH + * \overset{K_{IPA}}{\rightleftharpoons} (CH_3)_2CHOH*, \tag{8}$$

$$(CH_3)_2CHOH* + * \overset{k_1}{\rightarrow} (CH_3)_2CHO* + H*, \tag{9}$$

$$(CH_3)_2CHO* + * \overset{K_1}{\rightleftharpoons} (CH_3)_2CO* + H*, \tag{10}$$

$$(CH_3)_2CO* \overset{1/K_{Ace}}{\rightleftharpoons} (CH_3)_2CO + *, \tag{11}$$

$$2H* \overset{1/K_{H_2}}{\rightleftharpoons} H_2 + 2*, \tag{12}$$

where $*$ is an active site and K_i represents an adsorption equilibrium constant. If removal of the first hydrogen atom (hydroxyl hydrogen) is assumed to be an irreversible RDS, the rate of formation of acetone (Ace), r_{Ace}, is

$$r_{Ace} = Lk_1\theta_{IPA}\theta_v, \tag{13}$$

where L is the total number of active sites, k_1 is the forward rate constant of step 9, θ_{IPA} is the fractional coverage of isopropanol, and θ_v is the fraction of vacant sites.

The respective expressions for the quasi-equilibrated adsorption/desorption of IPA, hydrogen and acetone give

$$K_{\mathrm{IPA}} = \frac{\theta_{\mathrm{IPA}}}{P_{\mathrm{IPA}}\theta_{\mathrm{v}}}, \tag{14}$$

$$K_{\mathrm{H_2}} = \frac{\theta_{\mathrm{H}}^2}{P_{\mathrm{H_2}}\theta_{\mathrm{v}}^2}, \tag{15}$$

$$K_{\mathrm{Ace}} = \frac{\theta_{\mathrm{Ace}}}{P_{\mathrm{Ace}}\theta_{\mathrm{v}}}. \tag{16}$$

Study of the reaction orders showed that H_2 and acetone have a small inhibitory effect when added to the feed stream, and this leads to the inclusion of both hydrogen and acetone species in the site balance, along with molecularly adsorbed IPA. The presence of adsorbed IPA in the site balance was indicated by the in situ DRIFT spectrum obtained during IPA dehydrogenation. No isopropoxide species on the metal surface was included in the site balance because the IR spectra provided no evidence for its existence. Therefore, the site balance is

$$1 = \theta_{\mathrm{IPA}} + \theta_{\mathrm{H}} + \theta_{\mathrm{Ace}} + \theta_{\mathrm{v}}; \tag{17}$$

and utilization of Eqs. (14)–(17) gives

$$1 = K_{\mathrm{IPA}}P_{\mathrm{IPA}}\theta_{\mathrm{v}} + K_{\mathrm{H_2}}^{1/2}P_{\mathrm{H_2}}^{1/2}\theta_{\mathrm{v}} + K_{\mathrm{Ace}}P_{\mathrm{Ace}}\theta_{\mathrm{v}} + \theta_{\mathrm{v}}, \tag{18}$$

which yields

$$\theta_{\mathrm{v}} = \frac{1}{(1 + K_{\mathrm{IPA}}P_{\mathrm{IPA}} + K_{\mathrm{H_2}}^{1/2}P_{\mathrm{H_2}}^{1/2} + K_{\mathrm{Ace}}P_{\mathrm{Ace}})}. \tag{19}$$

Substitution of Eq. (19) and θ_{IPA} from Eq. (14) into Eq. (13) yields

$$r_{\mathrm{Ace}} = \frac{kK_{\mathrm{IPA}}P_{\mathrm{IPA}}}{(1 + K_{\mathrm{IPA}}P_{\mathrm{IPA}} + K_{\mathrm{H_2}}^{1/2}P_{\mathrm{H_2}}^{1/2} + K_{\mathrm{Ace}}P_{\mathrm{Ace}})^2}, \tag{20}$$

where $k = Lk_1$.

Eq. (20) was fitted to the experimental results with the use of Scientist, a commercially available data-fitting program, and to ensure that a global minimum had been obtained, an iterative process was initiated that used a number of different initial guesses for each value [31]. The optimized values for the four constants (k, K_{IPA}, $K_{\mathrm{H_2}}$, K_{Ace}) at four temperatures are listed in Table 10 for the monometallic Pt and the bimetallic Cu–Pt catalysts, and typical fits to experimental data are shown in Figs. 8–10 and 13–15. Similar fits were obtained with the other two catalysts [31]. Values for the rate constant k in Table 5 always increase with temperature, and equilibrium adsorption constants (K_i) always decrease, which is consistent with kinetic and thermodynamic expectations. Plots of $\ln K_i$ for species i versus $1/T$, shown in Figs. 17 and 18, yield values for $\Delta S^0_{\mathrm{ad},i}$, the standard entropy of adsorption, and $\Delta H^0_{\mathrm{ad},i}$, the standard enthalpy of adsorption, which are listed in Table 11. These values are physically meaningful because enthalpies are negative (exothermic adsorption), whereas entropies are also negative and less than the absolute entropy for each compound. The latter values satisfy all rules and guidelines provided to evaluate them [89,90]. This compliance does not guarantee that the proposed mechanism is correct, but it shows that it is thermodynamically consistent.

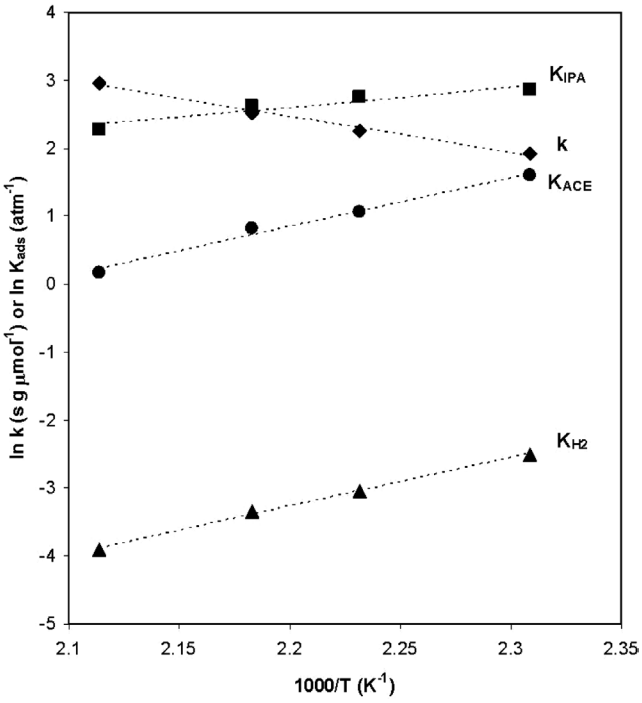

Fig. 17. Dependence of fitted parameters on temperature for 1% Pt/AC-HTT-H_2 reduced at 573 K.

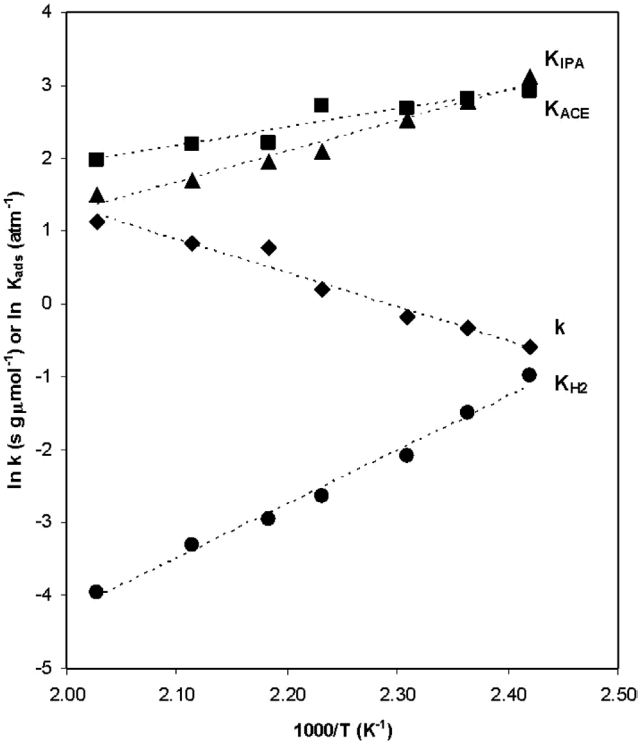

Fig. 18. Dependence of fitted parameters on temperature for 1% Cu-1% Pt/AC-HTT-H_2 reduced at 573 K.

Table 10
Kinetic parameters for IPA dehydrogenation on HTT-H_2 carbon-supported Pt and Cu–Pt catalysts after reduction at 573 K

Catalyst	T_{RXN} (K)	k[a] (μmol s^{-1} g^{-1})	K_{IPA} (atm^{-1})	K_{H_2} (atm^{-1})	K_{Ace} (atm^{-1})
1% Pt/AC-HTT-H_2	433	6.8	16.8	0.083	3.1
	448	9.5	16.0	0.046	2.5
	458	12.5	13.3	0.029	2.0
	473	19.2	9.6	0.021	1.7
0.5% Cu-1% Pt/AC-HTT-H_2	413	2.58	29.7	1.66	15.8
	423	3.35	24.7	0.94	13.8
	433	4.42	23.1	0.75	13.0
	448	6.57	16.0	0.60	10.5
	458	6.85	16.5	0.23	6.69
	473	8.68	13.2	0.14	2.94
	493	12.1	11.0	0.090	2.24
1% Cu-1% Pt/AC-HTT-H_2	413	0.49	23.5	0.88	23.0
	423	0.66	19.1	0.54	16.2
	433	0.85	16.8	0.38	12.5
	448	1.22	16.1	0.33	8.17
	458	2.09	12.3	0.16	6.39
	473	2.39	8.86	0.10	4.54
	493	2.92	6.92	0.07	2.96
5% Cu-1% Pt/AC-HTT-H_2	433	0.57	37.6	0.97	17.4
	448	0.85	34.1	0.70	16.0
	458	1.07	29.6	0.38	10.6
	473	1.80	17.2	0.25	6.5

[a] $k = Lk_1$.

Table 11
Thermodynamic parameters for IPA dehydrogenation on monometallic Pt and bimetallic Cu–Pt catalysts

Catalyst	E_{RDS} (kcal mol^{-1})	ΔH_{ads} (kcal mol^{-1})			ΔS_{ads} (cal mol^{-1} K^{-1})		
		IPA	H_2	Ace	IPA	H_2	Ace
1% Pt/AC-HTT-H_2	10.5	−5.8	−14.5	−6.4	−8	−34	−12
0.5% Cu-1% Pt/AC-HTT-H_2	7.7	−5.1	−15.1	−10.7	−6	−36	−20
1% Cu-1% Pt/AC-HTT-H_2	9.6	−6.1	−13.1	−10.1	−8	−32	−19
5% Cu-1% Pt/AC-HTT-H_2	11.5	−7.8	−14.6	−10.4	−10	−34	−18
1% Cu/AC-HTT-H_2[a]	22.9	−6.8	−13.4	−14.4	−8	−35	−24

[a] Taken from Ref. [4].

The heats of adsorption in Table 11 for Pt are in excellent agreement with integral heats of adsorption reported for Pt/SiO_2 catalysts [91] and with extrapolated integral heats of adsorption determined on various Pt single crystals [92–97]. The heat of adsorption for H_2 on Cu in Table 11 (13 kcal mol^{-1}) is somewhat lower than that for Pt, and the two catalysts with the most Cu have similar values of 13–14 kcal mol^{-1}. With two exceptions [98,99], 14 reported values for the heat of adsorption of H_2 on Cu surfaces have varied from 4 to 14 kcal mol [86,98–107], and thus the ΔH_{ad} values in Table 11 for H_2 on the Cu-containing catalysts are consistent with previous results. However, these values are more representative of low monolayer coverages of hydrogen, and H_2 adsorption on Cu is activated, in contrast to Pt. The heat of adsorption for IPA on the entire series of monometallic and bimetallic catalysts is low and ranges between 5 and 8 kcal mol^{-1}. Rendulic and Sexton measured a heat of adsorption of 12.6 kcal mol^{-1} for isopropanol on Pt(111) [108], and Vannice et al. reported a value of 12.1 kcal mol^{-1}, both in the low-coverage regime [11]. The heat of adsorption for acetone is lowest on Pt and highest on Cu, with the values for the bimetallic catalysts falling between the two respective values of 6 and 14 kcal mol^{-1}. These values are very reasonable compared with those measured for Cu and Pt single crystals; for example, Sexton and Hughes reported values of 10.1 and 11 kcal mol^{-1} for acetone on a Cu(110) and a Pt(111) surface, respectively [109], and Vannice et al. measured heats of adsorption of 11.5 and 12.6 kcal mol^{-1} for η^1 and η^2 bound acetone species, respectively [110]. Tripol'skii et al. have reported heats of adsorption of 19 and 9.2 kcal mol^{-1} for acetone on Cu/Cr_2O_3 and Cu/Al_2O_3, respectively [111]. The greater variation in the heat of adsorption for acetone could be due, at least partially, to the type of adsorbed species present. Even though the heat of adsorption is somewhat higher for acetone compared with IPA, the inhibitive effect of acetone is low be-

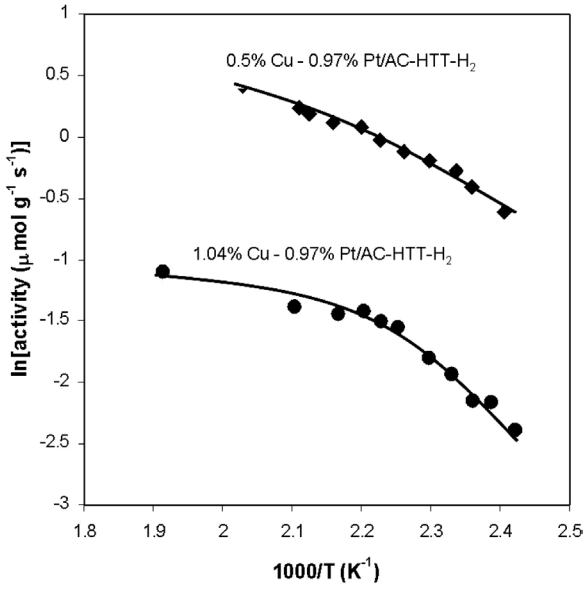

Fig. 19. Fit of Eq. (20) to activity data vs. $1/T$ for Cu–Pt/AC-HTT-H_2 catalysts.

cause of the high partial pressures of IPA in the feed and the low conversions, so that acetone partial pressures are low. DRIFT spectra for 1% Pt/AC-HTT-H_2 [31] and 0.5% Cu-1% Pt/AC-HTT-H_2 under reaction conditions suggest that IPA and acetone are adsorbed to the surface, and the shift in the absorption bands with respect to the vapor-phase values is very small, which is consistent with the evidence that IPA and acetone are weakly adsorbed. Similar fits to the kinetic data are obtained if the surface isopropoxide species is included in the site balance given by Eq. (17), and the only significant effect on the thermodynamic parameters is a decrease in the ΔH_{ad} and ΔS_{ad} values for acetone such that they become similar to those for IPA [31].

One difference in behavior provided by two of the bimetallic catalysts was a change in the apparent activation energy as the temperature increased. The bend-over in the Arrhenius plots for the 0.5% Cu-1% Pt/AC-HTT-H_2 and 1% Cu-1% Pt/AC-HTT-H_2 catalysts is not due to pore diffusion and suggests that either a change in the reaction mechanism occurred or a marked decrease in surface coverage of isopropanol took place as the temperature increased. The latter explanation appears to be the most appropriate, because the rate expression given by Eq. (20) actually provides the bend-over behavior observed, as shown in Fig. 19. Utilization of the K_i values in Table 10 allows one to calculate θ_{IPA} values, which decreased from 0.3 at 413 K to 0.1 at 493 K for the 1% Cu-1% Pt/AC-HTT-H_2 and compensated for the increase in the rate constant. Similar behavior has been observed for benzene hydrogenation over various metals [112–114], and in some cases the decreases in reactant surface coverage were so pronounced that apparent activation energies became negative.

5. Summary

Dehydrogenation of IPA over a family of carbon-supported Pt, Cu, and bimetallic Cu–Pt catalysts revealed that Pt was more active than copper and that all catalysts were 100% selective to acetone when supported on a high-temperature-treated carbon possessing no acidic surface groups. In contrast, a carbon support with a surface rich in acidic, oxygen-containing functional groups allowed a dehydration pathway to form propylene. Bimetallic Cu–Pt catalysts were less active than their monometallic counterparts on either a TOF or a weight basis, but they exhibited kinetic behavior similar to that of the monometallic catalysts. Bimetallic catalysts with Cu loadings of 1% or less displayed a change in apparent activation energy with temperature, and E_{app} decreased from 8.2 ± 1.0 to 3.4 ± 1.0 kcal mol^{-1} above 443 K. This decrease was not due to pore diffusional limitations, but was rather a kinetic effect due to the form of the rate expression. A Langmuir–Hinshelwood mechanism assuming that removal of the first hydrogen atom from the hydroxyl group was rate-determining fit the data well, provided physically and thermodynamically meaningful rate parameters, and explained the decrease in E_{app} at higher temperatures. In addition to hydrogen and acetone, which produced small rate inhibitions, inclusion of IPA in the site balance was supported by in situ diffuse-reflectance infrared spectra. The heats of adsorption for IPA, H_2, and acetone obtained from the adsorption equilibrium constants in the rate expression were consistent with values reported by surface science and adsorption studies.

Acknowledgment

This study was supported by the National Science Foundation via grant CTS-9903559.

References

[1] P. Fuderer-Luetić, I. Brihta, Croat. Chem. Acta 31 (1959) 75.
[2] I. Brihta, P. Luetić, Croat. Chem. Acta 29 (1957) 419.
[3] L.S. Vadlamannati, V.I. Kovalchuk, J.L. d'Itri, Catal. Lett. 58 (1999) 173.
[4] R.M. Rioux, M.A. Vannice, J. Catal. 216 (2003) 362.
[5] L.J. Shorthouse, A.J. Roberts, R. Raval, Surf. Sci. 480 (2001) 37.
[6] M. Weldon, C.M. Friend, Chem. Rev. 96 (1996) 1391.
[7] D.A. Chen, C.M. Friend, Langmuir 14 (1998) 1451.
[8] C.J. Houtman, M.A. Barteau, J. Catal. 130 (1991) 528.
[9] X. Xu, C.M. Friend, Surf. Sci. 260 (1992) 14.
[10] J.L. Davis, M.A. Barteau, Surf. Sci. 235 (1990) 235.
[11] M.A. Vannice, W. Erley, H. Ibach, Surf. Sci. 254 (1991) 12.
[12] S.V. Chong, M.A. Barteau, H. Idriss, Catal. Today 63 (2000) 283.
[13] R.L. Brainard, R.J. Madix, Surf. Sci. 214 (1989) 396.
[14] P.D.A. Pudney, S.A. Francis, R.W. Joyner, M. Bowker, J. Catal. 131 (1991) 104.
[15] I.E. Wachs, R.J. Madix, J. Catal. 53 (1978) 208.
[16] J. Zawadzki, M. Wiśniewski, J. Weber, O. Heintz, B. Azambre, Carbon 39 (2001) 187.
[17] Y. Han, J. Shen, Y. Chen, Appl. Catal. A 205 (2001) 79.

[18] K.C. Waugh, M. Bowker, R.W. Petts, H.D. Vandervell, J. O'Malley, Appl. Catal. 25 (1986) 121.
[19] D.E. Mears, M. Boudart, AIChE J. 12 (1966) 313.
[20] M. Kraus, Z. Žitnŷ, D. Mihajlova, A. Andreev, Collection Czechoslov. Chem. Commun. 41 (1976) 3563.
[21] G.S. Szymański, G. Rychlicki, Carbon 29 (1991) 489.
[22] R. Uma, J.C. Kuriacose, Ind. J. Chem. 10 (1972) 69.
[23] C.-Y. Shiau, S. Chen, J.C. Tsai, S.I. Lin, Appl. Catal. A 198 (2000) 95.
[24] H.Y. Chen, S.P. Lau, L. Chen, J. Lin, C.H.A. Huan, K.L. Tan, J.S. Pan, Appl. Surf. Sci. 152 (1999) 193.
[25] Y. Kanai, T. Watanabe, T. Fujitani, T. Uchijima, J. Nakamura, Catal. Lett. 38 (1996) 157.
[26] R. Burch, S.E. Golunski, M. Spencer, J. Chem. Soc., Faraday Trans. 86 (1990) 2683.
[27] R. Burch, S.E. Golunski, M. Spencer, Catal. Lett. 5 (1990) 55.
[28] G.J. Millar, C.H. Rochester, S. Bailey, K.C. Waugh, J. Chem. Soc., Faraday Trans. 88 (1992) 3497.
[29] N. Kanoun, M.P. Astier, G.M. Pajonk, Appl. Catal. 70 (1991) 225.
[30] A. Dandekar, R.T.K. Baker, M.A. Vannice, Carbon 36 (1998) 1821.
[31] R.M. Rioux, Master Thesis, The Pennsylvania State University, 2001.
[32] M.H. Kim, J.R. Ebner, R.M. Friedman, M.A. Vannice, J. Catal. 204 (2001) 348.
[33] M.H. Kim, M.A. Vannice, G.-D. Kim, J.-H. Lee, Korean J. Chem. Eng. 20 (2003) 247.
[34] M.H. Kim, J.R. Ebner, R.M. Friedman, M.A. Vannice, J. Catal. 208 (2002) 381.
[35] R.E. Rondeau, J. Chem. Eng. Data 11 (1966) 124.
[36] J.J. Venter, M.A. Vannice, Appl. Spec. 42 (1988) 1096.
[37] P.E. Fanning, M.A. Vannice, Carbon 31 (1993) 721.
[38] Handbook of X-Ray Photoelectron Data, Perkin-Elmer.
[39] N.W. Hurst, S.J. Gentry, A. Jones, Catal. Rev.-Sci. Eng. 24 (1982) 233.
[40] (a) P.B. Weisz, C.D. Prater, Adv. Catal. 6 (1954) 143;
(b) P.B. Weisz, Z. Phys. Chem. 11 (1957) 1.
[41] J. Ma, PhD Thesis, The Pennsylvania State University 1998.
[42] T. Shimanouchi, Tables of Molecular Vibrational Frequencies Consolidated Volume I, National Bureau of Standards, 1972.
[43] J. Ma, N.M. Rodriguez, M.A. Vannice, R.T.K. Baker, J. Catal. 183 (1999) 32.
[44] J. Ma, C. Park, N.M. Rodriguez, R.T.K. Baker, J. Phys. Chem. B 105 (2001) 11994.
[45] A. Dandekar, R.T.K. Baker, M.A. Vannice, J. Catal. 183 (1999) 131.
[46] M.B. Palmer Jr., M.A. Vannice, J. Chem. Tech. Biotechnol. 30 (1980) 205.
[47] V. Machek, J. Hanika, K. Sporka, V. Růžička, J. Kunz, Collection Czechoslov. Chem. Commun. 46 (1981) 3270.
[48] F. Coloma, A. Sepúlveda-Escribano, F. Rodríguez-Reinoso, J. Catal. 154 (1995) 299.
[49] M.C. Román-Martínez, D. Cazorla-Amorós, A. Linares-Solano, C. Salinas-Martínez De Lecea, H. Yamshita, M. Anpo, Carbon 33 (1995) 3.
[50] F. Rodríguez-Reinoso, I. Rodríguez-Ramos, C. Moreno-Castilla, A. Guerrero-Ruiz, J.D. López-González, J. Catal. 99 (1986) 171.
[51] D. Richard, P. Gallezot, in: B. Delmon, P. Grange, P.A. Jacobs, G. Poncelet (Eds.), Preparation of Catalysts IV, Elsevier, Amsterdam, 1987, p. 71.
[52] P. Ehrburger, O.P. Mahajan, P.L. Walker Jr., J. Catal. 43 (1976) 61.
[53] P. Ehrburger, P.L. Walker Jr., J. Catal. 55 (1978) 63.
[54] C. Prado-Burguete, A. Linares-Solano, F. Rodríguez-Reinoso, C. Salinas-Martínez De Lecea, J. Catal. 128 (1991) 397.
[55] A. Linares-Solano, F. Rodríguez-Reinoso, C. Salinas-Martínez De Lecea, O.P. Mahajan, P.L. Walker Jr., Carbon 20 (1982) 177.
[56] C. Prado-Burguete, A. Linares-Solano, F. Rodríguez-Reinoso, C. Salinas-Martínez De Lecea, J. Catal. 115 (1989) 98.
[57] V. Machek, B.N. Kuznetsov, Y.A. Ryndin, N.I. Kovalchuk, J. Chlebek, React. Kinet. Catal. Lett. 18 (1981) 253.
[58] J. Hanika, K. Sporka, V. Růžička, J. Bauer, Collection Czechoslov. Chem. Commun. 44 (1979) 2619.
[59] A.E. Aksoylu, M. Madalena, A. Freitas, M.F.R. Pereira, J.L. Figueiredo, Carbon 39 (2001) 175.
[60] L.R. Radovic, F. Rodríguez-Reinoso, Chem. Phys. Carbon 25 (1997) 243.
[61] D.J. O'Rear, D.G. Löffler, M. Boudart, J. Catal. 121 (1990) 131.
[62] M.H. Kim, M.A. Vannice, unpublished data, 2000.
[63] M.C. Román-Martínez, D. Cazorla-Amorós, A. Linares-Solano, C. Salines-Martínez De Lecea, Carbon 31 (1993) 895.
[64] A. Dandekar, M.A. Vannice, J. Catal. 178 (1998) 621.
[65] J.E. Benson, M. Boudart, J. Catal. 4 (1965) 704.
[66] C.A. Leon, M.A. Vannice, Appl. Catal. 69 (1991) 269.
[67] F. Epron, F. Gauthard, C. Pinéda, J. Barbier, J. Catal. 198 (2001) 309.
[68] B.D. Chandler, A.B. Schabel, L.H. Pignolet, J. Catal. 193 (2000) 186.
[69] N. Furuya, S. Motoo, J. Electroanal. Chem. 72 (1976) 165.
[70] B.C. Gates, J.R. Katzer, G.C.A. Schuit, Chemistry of Catalytic Processes, McGraw–Hill, New York, 1979.
[71] X. Wu, B.C. Gerstein, T.S. King, J. Catal. 121 (1990) 271.
[72] S.D. Robertson, B.D. Menicol, J.H. de Baas, S.C. Kloet, J. Catal. 37 (1975) 424.
[73] M. Boudart, M.A. Vannice, J.E. Benson, Z. Physik. Chem. N.F. 64 (1969) 171.
[74] W.C. Conner, J.L. Falconer, Chem. Rev. 95 (1995) 759.
[75] R.L. Augustine, Heterogeneous Catalysis for the Synthetic Chemist, Dekker, New York, 1996.
[76] W.G. Palmer, F.H. Constable, Roy. Soc. Proc. A. 106 (1924) 250.
[77] M. Kraus, in: G. Ertl, H. Knozinger, J. Weitkamp (Eds.), Handbook of Heterogeneous Catalysis, vol. 4, Wiley–VCH, Weinheim, 1997, p. 2159.
[78] B. Echevin, S.J. Teichner, Bull. Soc. Chim. Fr. 7 (1975) 1495.
[79] G. Djega-Mariadassou, A.R. Marques, L. Davignon, J. Chem. Soc. Faraday Trans. I 78 (1982) 2447.
[80] J.H. Sinfelt, J.L. Carter, D.J.C. Yates, J. Catal. 24 (1972) 283.
[81] J.H. Sinfelt, Bimetallic Catalysts, Wiley, New York, 1983.
[82] P.-A.D. Gaspillo, L.C. Abella, S. Goto, J. Chem. Eng. Japan 31 (1998) 440.
[83] P. Gastauer, M. Prevost, J. Chem. Eng. Japan 26 (1993) 580.
[84] Y. Ando, X. Li, E. Ito, M. Yamashita, Y. Saito, in: T. Inui (Ed.), New Aspects of Spillover Effect in Catalysis, Elsevier, Amsterdam, 1993, p. 313.
[85] E. Ito, M. Yamashita, S. Hagiwara, Y. Saito, Chem. Lett. 23 (1994) 351.
[86] E. Shustorovich, Surf. Sci. Report 6 (1986) 1.
[87] F.A. Carey, R.J. Sunberg, Advanced Organic Chemistry A, third ed., Plenum, New York, 1990.
[88] D.R. Lide (Ed.), CRC Handbook of Chemistry and Physics, seventy-third ed., CRC Press, Boca Raton, FL, 1992.
[89] M. Boudart, AIChE J. 18 (1972) 465.
[90] M.A. Vannice, S.H. Hyun, B. Kalpacki, W.C. Liauh, J. Catal. 56 (1979) 358.
[91] B. Sen, P. Chou, M.A. Vannice, J. Catal. 101 (1986) 517.
[92] R.W. McCabe, L.D. Schmidt, in: Proceedings, 7th International Vacuum Congress, Vienna, 1997, p. 1201.
[93] P.R. Norton, J.A. Davies, T.E. Jackman, Surf. Sci. 121 (1982) 103.
[94] K. Christmann, G. Ertl, T. Pignet, Surf. Sci. 54 (1976) 365.
[95] P.R. Norton, P.J. Richards, Surf. Sci. 44 (1974) 129.
[96] I. Toyashima, G. Somorjai, Catal. Rev.-Sci. Eng. 19 (1979) 105.
[97] S. Cerny, M. Smutek, F. Buzek, J. Catal. 38 (1975) 245.
[98] M.D. Malev, Sov. Phys.-Tech. Phys. 17 (1973) 2009.
[99] J.M. Campbell, C.T. Campbell, Surf. Sci. 259 (1991) 1.
[100] J. Pritchard, F.C. Tompkins, Trans. Faraday Soc. 56 (1960) 540.
[101] C.S. Alexander, J. Pritchard, J. Chem. Soc. Faraday Trans. I 68 (1972) 202.
[102] J. Pritchard, T. Catterick, R.K. Gupta, Surf. Sci. 53 (1975) 1.
[103] M. Balooch, M.J. Cardillo, D.R. Miller, R.E. Stickney, Surf. Sci. 46 (1974) 358.
[104] G. Ander, A. Winkler, K.D. Rendulic, Surf. Sci. 220 (1989) 1.

[105] M.J. Sandoval, A.T. Bell, J. Catal. 144 (1993) 227.
[106] J. Tabatabaei, B.H. Sakakini, M.J. Watson, K.C. Waugh, Catal. Lett. 59 (1999) 151.
[107] H. Wilmer, T. Genger, O. Hinrichsen, J. Catal. 215 (2003) 188.
[108] K.D. Rendulic, B.A. Sexton, J. Catal. 78 (1982) 126.
[109] B.A. Sexton, A.E. Hughes, Surf. Sci. 140 (1984) 227.
[110] M.A. Vannice, W. Erley, H. Ibach, Surf. Sci. 254 (1991) 1.
[111] A.I. Tripol'skii, N.V. Pavalenko, G.I. Godolets, Kinet. Catal. 26 (1985) 976.
[112] R.Z.C. van Meerten, J.W.E. Coenen, J. Catal. 46 (1977) 13.
[113] H. Kubicka, J. Catal. 12 (1968) 223.
[114] K.J. Yoon, M.A. Vannice, J. Catal. 82 (1983) 457.